Quaternary Science Reviews 324 (2024) 108443

Contents lists available at ScienceDirect

Quaternary Science Reviews

journal homepage: www.elsevier.com/locate/quascirev

Ice core evidence for an orbital-scale climate transition on the Northwest Tibetan Plateau

L.G. Thompson [a,b,*], T.-D. Yao [c], M.E. Davis [a], E. Mosley-Thompson [a,d], H.-A. Synal [e], G. Wu [c], J.F. Bolzan [a], S. Kutuzov [a,b], E. Beaudon [a,b], M.R. Sierra-Hernández [a], J. Beer [e]

[a] Byrd Polar and Climate Research Center, The Ohio State University, Columbus, OH, 43210, USA
[b] School of Earth Sciences, The Ohio State University, Columbus, OH, 43210, USA
[c] Key Laboratory of Tibetan Climate Changes and Land Surface Processes, Institute of Tibetan Plateau Research, Chinese Academy of Sciences, Beijing, China
[d] Department of Geography, The Ohio State University, Columbus, OH, 43210, USA
[e] Laboratory of Ion Beam Physics, ETH Zurich, Otto-Stern-Weg, 58093, Zurich, Switzerland

ARTICLE INFO

Handling Editor: Dr A. Voelker

Original content: Guliya Ice Cap, China, -0.064 41ka BP stable isotope, NH4, dust data (Original data)

Keywords:
Ice core
Northwest Tibetan plateau
Orbital forcing
Glacial stage
Holocene
Indian summer monsoon
Westerlies
Oxygen isotopes

ABSTRACT

The influences on climate in the Northwest Tibetan Plateau (NwTP) have changed on millennial to precessional timescales and have been dependent on the size of the Northern Hemisphere ice sheets, Northern Hemisphere summer insolation, and the migration of the Intertropical Convergence Zone (ITCZ). All these influences control the position and intensity of the westerlies over Central Asia and the Tibetan Plateau and of the Asian Monsoon over South Asia. The top 187.4 m of a 309.7-m ice core (2015GP) drilled on the plateau of the Guliya ice cap contains a 41-kyr climate history of the NwTP, a region where information on past climate and environment is limited. The oxygen isotope ratio ($\delta^{18}O$), and ammonium (NH_4^+) and dust concentration records from 2015GP show that during the glacial (41–17.5 ka BP) temperature and precipitation in the NwTP were primarily influenced on the precessional timescale by summer insolation, while at millennial resolution the climate was linked to the North Atlantic temperature via the westerlies. During the deglaciation (17.5–12 ka BP) summer insolation remained an important temperature forcing, but the influence of the North Atlantic climate on the NwTP climate weakened as the westerlies shifted northward. The Guliya Holocene $\delta^{18}O$ record shows that NwTP climate was no longer in phase with decreasing summer insolation or with North Atlantic climate, perhaps as the moisture source and pathways were more determinative factors in isotopic fractionation than temperature, and/or incoming solar radiation (insolation) forcing was replaced by rising greenhouse gas concentrations as the primary driver of warming in NwTP.

1. Introduction

The Tibetan Plateau (TP) and its surrounding mountain ranges, collectively known as the Third Pole, contain the largest mass of ice outside the polar regions. The glaciers and ice sheets in the Third Pole provide a vital source of water for almost a billion people from Central to South Asia (Pritchard, 2019) and the recent warming since the middle of the 20th century has become an increasing threat to the cryosphere and hydrosphere of this vast region (Kraaijenbrink et al., 2017; Yao et al., 2020). In response to this warming, glaciers in the Himalayas and in the southern TP have receded at significant and increasing rates over the last 50 years (Yao et al., 2020); however, until recently glaciers in the Northwest Tibetan Plateau (NwTP) have gained mass or remained stable (Farinotti et al., 2020). This slight increase in the NwTP glacier budget has been attributed to the recent increase in precipitation (Yao et al., 2012; Thompson et al., 2018), particularly during the ablation season (Zhu et al., 2022) and/or a regional warming hiatus from 2001 to 2012 (An et al., 2016). However, since 2015 the increase in ice accumulation has ceased (Hugonnet et al., 2021). High Asia is warming faster than much of the rest of the world, and projections of a global temperature increase of 1.5 °C may result in a mass loss of the region's glaciers of 49 ± 7% to 64 ± 5% (the end members of the IPCC Representative Concentration Pathways) by the end of the 21st century (Kraaijenbrink et al., 2017).

In addition to its high altitude and diverse geomorphology, the Third Pole is a region of complex climatology where air masses from multiple

* Corresponding author. Byrd Polar and Climate Research Center, The Ohio State University, Columbus, OH, 43210, USA.
E-mail address: thompson.3@osu.edu (L.G. Thompson).

https://doi.org/10.1016/j.quascirev.2023.108443
Received 11 August 2023; Received in revised form 27 November 2023; Accepted 27 November 2023
Available online 9 December 2023
0277-3791/

sources interact on seasonal to orbital timescales (Maussion et al., 2014; Yao et al., 2012, 2013; Cheng et al., 2012, Cheng et al., 2016a; Hou et al., 2017; Thompson et al., 2018, Thompson et al., 2022). The relationship between North Atlantic temperature, the westerly jet, and the strength of the Asian monsoon is well established (Burns et al., 2003; Gupta et al., 2003; Goswami et al., 2006; Feng and Hu, 2008; Deplazes et al., 2013; Marzin et al., 2013; Tierney et al., 2016), although disparities exist among the proposed mechanisms linking the oceanic/atmospheric processes of the North Atlantic and Asia. Modern climate and paleoclimate records show that on decadal and longer timescales warming (cooling) in the North Atlantic is connected to stronger (weaker) monsoon circulation through modulation of the westerly jet. This close association between the westerly jet and the Asian Monsoon determines precipitation patterns and intensity on the TP and in arid Central Asia. Paleoclimate records from the North Atlantic, specifically $\delta^{18}O$ from Greenland ice cores such as GISP2 (Grootes and Stuvier, 1997) show consistent relationships with records of Asian monsoon intensity (Deplazes et al., 2013; Dutt et al., 2015; Cheng et al., 2016b).

Today the westerlies and local recycling appear to be the dominant influence on the climate of the northern TP (Curio et al., 2015; An et al., 2017); however, several studies conclude that in the past the Indian summer monsoon (ISM) may have played a more important role (Cheng et al., 2012; Cheng et al., 2016a; Ramisch et al., 2016; Hou et al., 2017; Thompson et al., 2022). The relative importance of tropical and polar air masses on the TP has changed depending on conditions that include the extent of the Northern Hemisphere ice sheets, the latitudinal thermal gradient, and the position of the intertropical convergence zone (ITCZ) (Arbuszewski et al., 2013; Deplazes et al., 2013; Zhu et al., 2015; Thomas et al., 2016; Ramisch et al., 2016; Hou et al., 2017; Hari et al., 2020; Thompson et al., 2022). The complex interplay of air masses on the Tibetan Plateau on decadal to orbital time scales complicates efforts to reconstruct the regional climate history and atmospheric dynamics.

2. Materials and methods

2.1. Study area and ice core drilling program

The western Kunlun Mountains are located in the NwTP along the southern rim of the Tarim Basin and adjacent to the Karakoram Mountains to the west (Fig. 1A) and lie north of the transitional regime between the westerlies and the ISM influence (Yao et al., 2013). The boundary between these regimes shifts latitudinally depending on the position of the subtropical westerly jet (Zhu et al., 2021), which influences the variability of seasonal precipitation on the Tibetan Plateau and in Central Asia (Schiemann et al., 2009). The Kunlun Mountains contain numerous peaks over 6000 masl and one of the largest concentrations (537 glaciers >0.02 km^2 with a total area of 3137 km^2) of "polar-type" glaciers (Cao et al., 2020) outside the polar regions (Ke et al., 2015). Among the largest of the ice masses in the Kunlun Mountains is the western Kunlun ice sheet (Fig. 1A), over which annual precipitation varies between 24 and 400 mm (Huang et al., 2019). The meltwater from the Kunlun ice sheet is a primary source of water for the rivers in the Tarim Basin that support agriculture and economic development (Disse, 2016).

The Guliya ice cap (35.25°N; 81.48°E), the largest glacier (376 km^2) in the western Kunlun range (Kutuzov et al., 2018), is located on the southern slope of this mountain range (Fig. 1B). The elevation of the Guliya summit (GS) is 6710 masl, and below the summit is a large, flat ice plateau (6200 masl) (Fig. 1C). The thickness of the ice at the summit is ~51 m, and the maximum ice thickness on the Guliya plateau (GP) is ~370 m (Kutuzov et al., 2018). Estimates of the amount of annual precipitation received by the ice cap in recent decades vary between 106 and 428 mm w. e. a^{-1} (Kutuzov et al., 2018; Thompson et al., 2018; Zhu et al., 2022). Like the rest of the western Kunlun ice sheet, Guliya is a polar-type glacier which is frozen at the base (Thompson et al., 2018).

A drilling program on the Guliya plateau in the summer of 1992 resulted in the recovery of a 308.6-m ice core to bedrock (1992GP) from which a >110 kyr climate record was reconstructed (Thompson et al.,

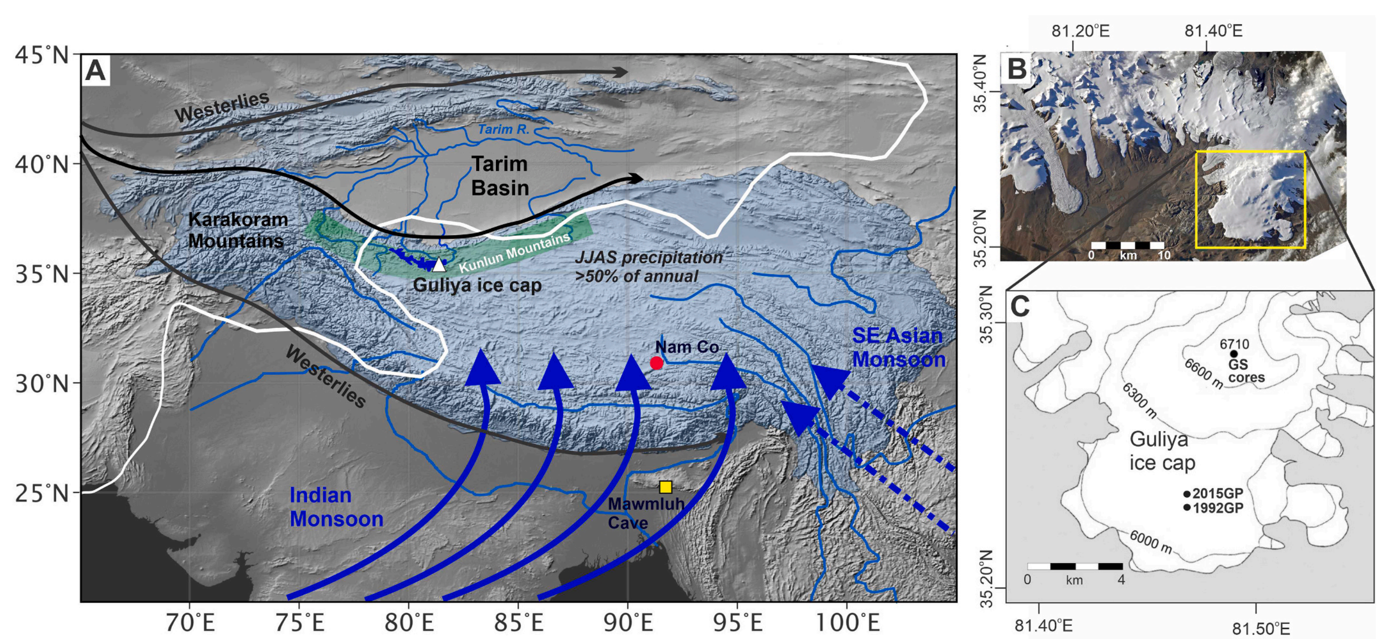

Fig. 1. Geographic and climatological settings of Guliya ice cap (A) Relief map of the Tibetan Plateau (highlighted in light blue) showing the major air masses, along with the locations of the Guliya ice cap (white filled triangle) in the western Kunlun ice sheet (highlighted in darker blue), Nam Co (red filled circle) and the Mawmluh Cave (yellow filled square). The white line defines the area of summer (JJAS) precipitation dominance from 2010 to 2022 (data from https://iridl.ldeo.columbia.edu/SOURCES/.NOAA/.NCEP-NCAR/.CDAS-1/.MONTHLY/.Diagnostic/.surface/.prate/). (B) Satellite image of the southeast sector of the western Kunlun ice sheet. The Guliya ice cap is outlined by the yellow box. (C) A topographic map shows the locations of the 1992 and 2015 drill sites on the Guliya plateau (1992GP, 2015GP) and the 2015 drill sites on the Guliya summit (GS cores).

1997). The time series of stable isotopes of oxygen ($\delta^{18}O$) from 1992GP shows orbital-scale similarities with polar ice core records of methane (CH_4) concentrations, which suggests linkages between the subtropical hydrological cycle and global CH_4 variations. In 2015 a second drilling program on Guliya yielded a 309.7 m core from the GP (2015GP) and, for the first time, three cores were drilled to bedrock (GS1: 50.72 m, GS2: 51.38 m, and GS3: 50.86 m) on the GS (Fig. 1C). The 2015GP borehole was located very close to that for the 1992 core (35.233°N; 81.468°E and 35.227°N; 81.468°E, respectively) (Fig. 1C). The results of a ground-penetrating radar survey conducted on the GP during the 2015 drilling program revealed rugged bedrock topography below the ice cap, with both boreholes located within a U-shaped subglacial valley (Kutuzov et al., 2018).

The climatic and environmental records from 1840 to 2014 CE in the 2015GP and GS ice cores were discussed in Thompson et al. (2018), and Thompson et al. (2022) presented the time series of $\delta^{18}O$ and deuterium excess for the last 15 kyr that were constructed with the aid of $\delta^{18}O_{atm}$ (stable isotope ratios of oxygen in entrapped air) measurements on one of the GS cores, a method rarely used on nonpolar ice cores. Here, we extend the climate record from the 2015GP core back to 41 ka BP, or the late Marine Isotope Stage 3 (MIS3), using records of stable water isotopes, ammonium (NH_4^+) and insoluble dust concentrations, and the concentrations of cosmogenic isotopes Beryllium-10 (^{10}Be) and Chlorine-36 (^{36}Cl) to aid in timescale development. This facilitated an evaluation of how variations in the intensities and positions of mid-latitude and tropical air masses influence the climate of the NwTP on millennial to precessional timescales.

2.2. Laboratory analysis of ice cores

The entire length of the 2015GP core (9329 samples) was analyzed for $\delta^{18}O$, hydrogen isotopes (δD), insoluble dust concentrations and size distributions between 0.63 and 16 μm diameter, and for concentrations of major cations (Na^+, NH_4^+, K^+, Mg^{2+}, Ca_2^+), and anions (F^-, Cl^-, SO_4^{2-}, NO_3^-). The stable water isotope (^{16}O, ^{18}O, H^1, and H^2 or D) measurements were made using a Picarro cavity ring-down spectrometer (L2120-i), with an average precision of 0.25‰ for $\delta^{18}O$ and 0.80‰ for δD. Deuterium excess (d-excess) was calculated by the function [d-excess = δD - ($8 \times \delta^{18}O$)]. Major ion concentrations were measured with a Thermo Scientific Dionex ion chromatograph ICS-5000. The very high dust concentrations in the Guliya ice necessitated the dilution of the melted ice core samples with ultra-pure Milli-Q water prior to measurement using a Beckman Coulter Multisizer 4 equipped with a 30 μm aperture tube. Mineral dust concentrations were measured in 14 size bins between 0.63 and 16 μm diameter.

2.3. Time scale reconstruction

The construction of the timescales for the last 15 kyr of the Guliya plateau and summit ice core records is described in Thompson et al. (2022). In brief, a timescale was developed for summit core GS3 using: 1) layer-counted years in 2015GP determined from seasonal variations of $\delta^{18}O$ and aerosols back to 0.11 ka BP (relative to 1950 CE); 2) radiocarbon dates from plant fragments in 2015GP and GS2, and 3) measurements $\delta^{18}O_{atm}$ in GS3. Measurement of $\delta^{18}O_{atm}$ in samples from GS3 was possible because a 25-m firn layer exists at the summit; however, no firn layer is preserved on the GP where the snowfall metamorphoses into ice within a year of deposition (Thompson et al., 2022). By transferring the layer counted years at the top of 2015GP (Thompson et al., 2018) and the ^{14}C ages from 2015GP and GS2 to GS3 by $\delta^{18}O$ matching, a 15 kyr timescale was developed for the top ~50 m of the 50.86 m long GS3 core. This was transferred by $\delta^{18}O$ matching to the top 144 m of the 309.7 m long 2015GP core. This match provides strong evidence that the ages of 1992GP and 2015GP are older than the late deglaciation (~11.7–~15 ka BP), thus challenging suggestions that 1992GP does not extend beyond the Holocene (Hou et al., 2018, 2019).

To extend the timescale before 15 ka BP, 34 samples from 2015GP ranging from 1.0 to 4.2 m in length were measured for concentrations of the cosmogenic isotopes ^{10}Be and ^{36}Cl (Fig. 2A), using the methodology described by Beer et al. (2012). Two peaks in both isotopes appear between 175 and 190 m (Fig. 2B). A prominent ^{36}Cl signal was observed in the 1992GP core at 183.6 m (Fig. 2C) (Thompson et al., 1997), and the cosmogenic isotope data from 2015GP confirmed this ^{36}Cl peak, along with a peak in ^{10}Be, at 187.4 m. This cosmogenic isotope signal, known as the Laschamp Event (LE), has been observed in ^{10}Be concentrations in polar ice cores (Muscheler et al., 2005; Svensson et al., 2006; Raisbeck et al., 2017), marine sediments (Channell, 2006; Liu et al., 2020), lake basin sediments (Nilsson et al., 2011; Belmaker et al., 2014), and Chinese loess sequences (Pan et al., 2002; Zhou et al., 2007; An et al., 2014). These sources provide an age range for the LE of 37–42 ka BP; however, many studies fix the main phase of the event at ~41 ka BP (Svensson et al., 2006; Roberts, 2008; Lascu et al., 2016; Panovska et al., 2021).

Another $^{36}Cl/^{10}Be$ peak centered at 179 m occurs in 2015GP (Fig. 2B) but was not detected in 1992GP due to lower sampling resolution in that core. This peak may mark the Mono Lake Event (MLE), the age of which is controversial and difficult to define. Although the existence of the MLE has been disputed (Kent et al., 2002), several studies have dated it between ~30 ka BP and ~36 ka BP (Wagner et al., 2000; Pan et al., 2002; Benson et al., 2003; Channell, 2006; Cassata et al., 2008; Laj et al., 2014; Korte et al., 2019; Liu et al., 2020). Several ^{10}Be peaks occur in the Greenland GRIP ice core between 31 and 38 ka BP, although none were distinguishable as the MLE (Svensson et al., 2006). The LE and the MLE appear to be two distinct events in 2015GP (Fig. 2B), and for this study the age of the younger is fixed at 33 ka BP which is the average of the ages of the MLE in the references listed in Table 1. A major caveat is that the MLE may have been either a very long duration event or a series of small excursions that lasted thousands of years.

With the most recent 15 kyr of the 2015GP timescale already established and presented by Thompson et al., (2022), the chronology from 15 ka BP to 41 ka BP was developed using a 3rd order polynomial function based on the age/depth every 100 years from 13.9 to 15 ka BP and the age/depth of the LE (41 ka BP/187.4 m) and MLE (33 ka BP/179 m) cosmogenic isotope peaks (Fig. 3). As the ice core record lacks evidence of known dated events between 15 and ~33 ka BP that could be used to constrain the function and because the age of the MLE is controversial, the polynomial-derived timescale potentially contains uncertainties of several hundred years between 15 and ~33 ka BP. However, the 2015GP and GISP2 $\delta^{18}O$ records are reasonably matched where chronological control is available during the glacial (i.e., ~33 and 41 ka BP) (Supplement Fig. S1). To refine the timescale between 15 and 33 ka BP, the glacial stage portion of the 2015GP $\delta^{18}O$ record (17.5–41 ka BP) was detrended to remove orbital oscillations and tuned to the detrended $\delta^{18}O$ record from the Greenland GISP2 ice core record using Analyseries (Paillard et al., 1996) with the ages of the LE and MLE as control points. The resulting match between the detrended $\delta^{18}O$ records from 15 to 41 ka BP is shown in Supplement Fig. S2. The time/depth relationship resulting from this isotopic matching is shown by the black curve in Fig. 3.

3. Results

3.1. The 41 kyr Guliya record

The top 187.4 m of $\delta^{18}O$, NH_4^+, mineral dust concentrations, and d-excess in 2015GP are shown by depth in Fig. 4, with age intervals depicted along the top x-axis. Prominent precession-scale oscillations occur below ~130 m (~10 ka BP) in the $\delta^{18}O$, NH_4^+, and dust concentration records (Fig. 4A–C). The d-excess data contain features that align with the other profiles; however, they show an overall decreasing trend throughout the 41 kyr record. The gray bar in Fig. 4 between 60 and 70 m marks the location of nearly dust- and bubble-free ice along with

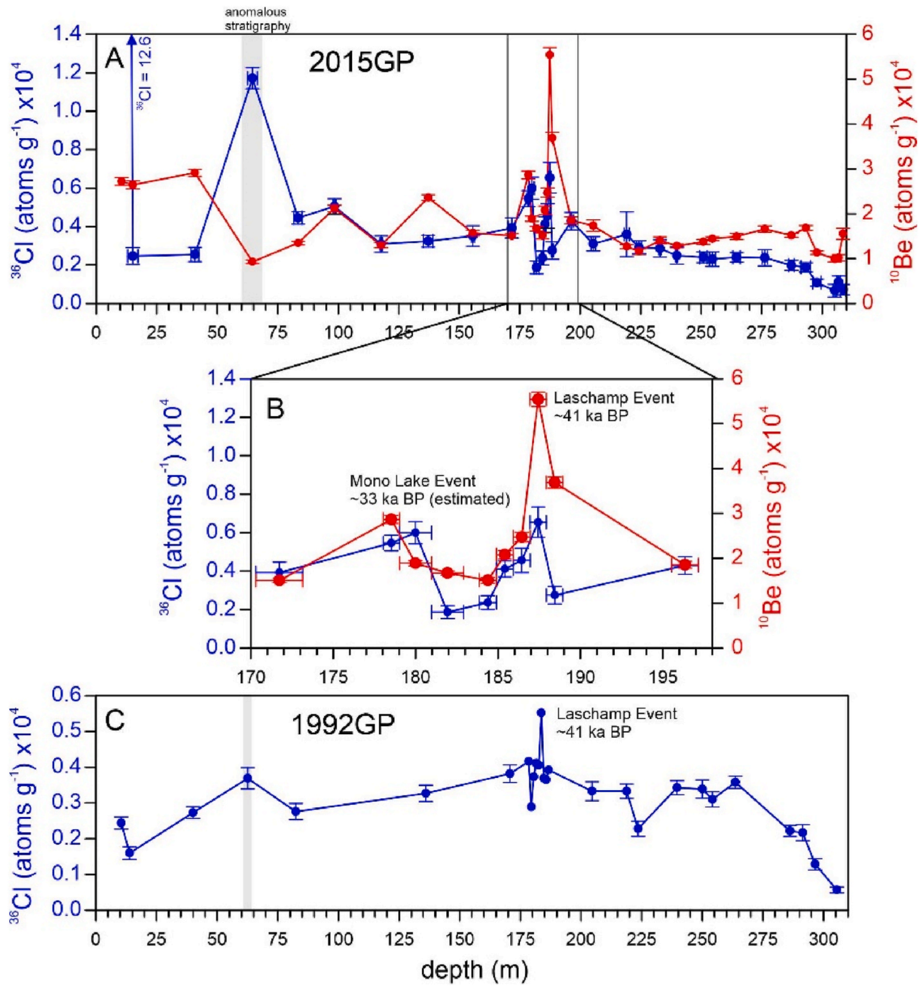

Fig. 2. Cosmogenic isotopes in Guliya Plateau cores. (A) ^{36}Cl (blue plot) and ^{10}Be (red plot) measurements in 2015GP. The outlined portion is expanded (B) to show the cosmogenic isotope peaks at ~179 m (possible Mono Lake Event) and 187.4 (Laschamp Event). (C) The ^{36}Cl profile in 1992GP shows a peak at 184 m which marks the Laschamp Event (Thompson et al., 1997). Gray bars in (A) and (C) indicate intervals in the cores in which the physical and chemistry stratigraphies are anomalous and may be the result of crevasse fill. The anomalous ice layer in 2015GP is thicker than in 1992GP. Upward-oriented arrow in (A) indicates a ^{36}Cl concentration (12.6) that exceeds the upper limit of the y-axis value.

Table 1
Proposed ages of the Mono Lake Event.

Location	Age of the MLE	Source
French Chaîne des Puys	34.2 ± 1.2	Laj et al. (2014)
Pyramid Lake Basin, Nevada	32.4 ± 0.9	Benson et al. (2003)
Auckland volcanic field, New Zealand	31.6 ± 1.8	Cassata et al. (2008)
Santa Clara Valley, California	32.8 ± 0.33	Mankinen and Wentworth (2004)
Spherical harmonic field modeling	30–36	Korte et al. (2019)
Black Sea	~34.5	Liu et al. (2020)
Irminger Basin, North Atlantic	32–34	Channell (2006)
Greenland Summit	~32	Wagner et al. (2000)

lower δ^{18}O and high d-excess values and three peaks in NH_4^+ concentration. This interval, which is dated between 0.25 and 0.45 ka BP, also contains a very high concentration of ^{36}Cl (Fig. 2A). A similar but smaller layer of ice, also shaded in gray in Fig. 4, occurs between 87 and 89 m. The 1992GP ice core also contains stratigraphically anomalous ice between 60 and 64 m along with a large ^{36}Cl concentration (gray shading in Fig. 2C). This ^{36}Cl peak in 2015GP differs from others in the core because it is not accompanied by an increase in ^{10}Be (^{10}Be was not measured in the 1992GP core). The origin of this ice with unusual physical and chemical characteristics is unknown; however, one possibility involves Guliya's location in an active seismic zone. Large earthquakes have been observed in the area, and a recent example is a magnitude 7.1 tremor in 2008 (the Yutian earthquake) that originated in a fault just north of the ice cap and produced a 31 km long rupture zone (Xu et al., 2013). It is possible that at some time around the middle of the 20th century such a quake opened a crevasse in the GP near the location of the boreholes. This crevasse may subsequently have received precipitation that was contaminated with ^{36}Cl, a large quantity of which was produced by marine testing of nuclear weapons in the 1950s. The shallowest sample from 2015GP (9–12 m depth) contains a ^{36}Cl concentration of 12.6×10^4 atoms g^{-1} (Fig. 2A) which is comparable to the average ^{36}Cl concentration in the mid-1960s in a shallow core from Greenland (Elmore et al., 1982).

3.1.1. Influences on Guliya stable isotopes and potential sources of ammonium

Stable isotopes of water in polar precipitation have traditionally been interpreted as proxies for temperature (Johnsen et al., 2001; Masson-Delmotte et al., 2008). However, in lower latitude regions such as the TP the influences on isotopic fractionation are more complex (Vuille et al., 2005; Yao et al., 2013). Several decades of research on the hydrologic cycle and cryosphere of the TP have provided a large body of

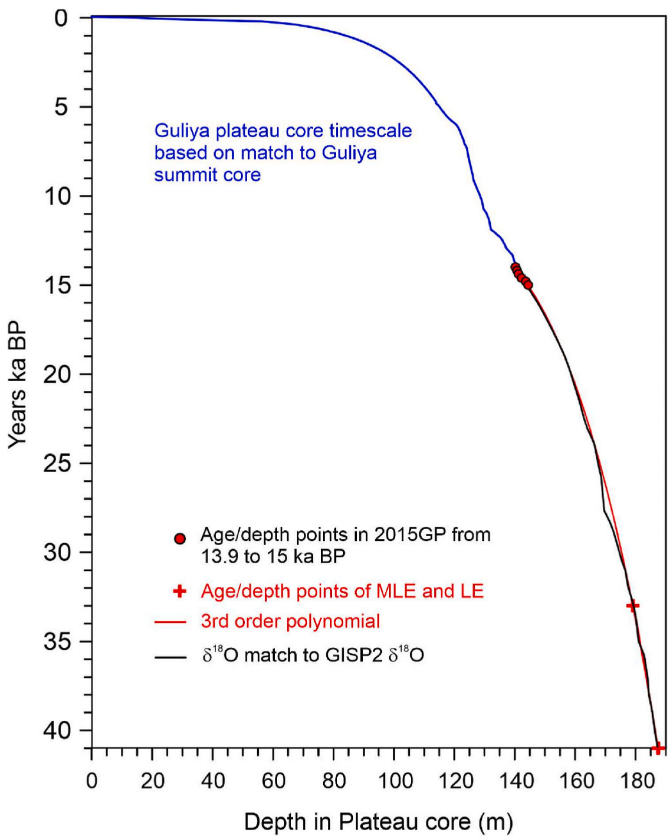

Fig. 3. Time/depth curve for the upper 187.4 m of 2015GP. The interval from 0 to 144 m (blue curve) is based on a $\delta^{18}O$ match between 2015GP and a $\delta^{18}O_{atm}$ and ^{14}C dated core from the GS (Thompson et al., 2022). From 144 to 187.4 m the timescale is determined by a 3rd order polynomial (red curve) pinned to the time/depth points between 13.9 and 15 ka BP (black bordered red circles) and the Mono Lake and Laschamp Events (red crosses). The black curve over this interval is the result of glacial stage matching of the 2015GP and GISP2 $\delta^{18}O$ records.

data on stable isotopes in precipitation and their use in constructing paleoclimate records, primarily from ice cores, lake sediments, speleothems, and biological material. In the northern TP significant seasonal to decadal correlations between air temperature and $\delta^{18}O$ in precipitation have been demonstrated (Yao et al., 1996, 2013; Tian et al., 2003, 2007; Thompson et al., 2018). This recent correlation was assumed to extend back through at least the Holocene, resulting in the reconstruction of temperature histories from ice core $\delta^{18}O$ records collected from glaciers in the northern TP (Wang et al., 2006; An et al., 2016; Thompson et al., 1997, Thompson et al., 2006, 2018; Tian et al., 2006; Pang et al., 2020; Yu et al., 2021). However, recent work on stable isotopes in TP precipitation shows that the atmospheric and hydrospheric influences on $\delta^{18}O$ and hydrogen isotopes (δD) are more complex than previously thought, including in regions near the NwTP where moisture is derived from continental and tropical air masses and local sources. In addition to temperature, these influences include precipitation source, isotopic fractionation at the source, convective vs. stratiform cloud cover, transport pathways (i.e., over land vs. water), and altitude (Pang et al., 2011; Yao et al., 2013; Aggarwal et al., 2016; Han et al., 2016). The effects of each of these processes on $\delta^{18}O$ in the NwTP may vary through time as tropical and westerly air masses migrate along with westerlies and monsoons (Thompson et al., 2022).

Studies of d-excess in recent precipitation and glacier ice on the TP and in Central Asia demonstrate that its value can be affected by both local and large-scale processes (An et al., 2017; Bershaw, 2018; Kreutz et al., 2003). An et al. (2017) used isotope modeling on data from the Chongce glacier in the western Kunlun ice sheet near the Guliya ice cap to determine that almost half of the precipitation in the NwTP comes from local recycling which increases with rising temperatures. However, d-excess may also be affected by changes in large-scale atmospheric circulation and thus moisture source (An et al., 2017; Bershaw, 2018). High values in TP precipitation are associated with very high d-excess moisture from the Mediterranean, which recycles over Central Asia, but d-excess can be reduced by mixing with moisture from other sources, such as the Indian Ocean (An et al., 2017; Bershaw, 2018).

Ammonium (NH_4^+) is formed by the reaction between ammonia (NH_3), one of the most abundant bases in the atmosphere, and H_2SO_4 and HNO_3 acids, which are converted to $(NH_4)_2SO_4$, NH_4HSO_4 and

NH_4NO_3 respectively. NH_4^+ measured in ice serves as a proxy for NH_3. Although over the last two centuries anthropogenic activities such as farming and animal husbandry have dominated NH_3 emissions, natural sources for NH_4^+ in the atmosphere include biological activity in soils, vegetation, wetlands, and water (Bouwman et al., 1997; Aneja et al., 2001; Chen et al., 2021). For example, NH_4^+ measured in the Illimani ice core from the Bolivian Andes most likely originated from soil and vegetation in the nearby Amazon Basin (Kellerhals et al., 2010). Potential sources of NH_4^+ found in the Guliya ice cap include large bodies of water to the west such as the Caspian and Black Seas and lakes and wetlands in Central Asia and in the TP that have expanded and receded through time (Herzschuh, 2006; Koriche et al., 2022). The use of NH_4^+ as a proxy for variations in available water in and around the NwTP is supported by the record of dust concentrations in 2015GP, which shows opposite trends to ammonium, particularly before 10 ka BP (Fig. 4B and C). High NH_4^+ and low dust concentrations together suggest expanded water surface area and an overall wetter climate that helped minimize dust sources.

3.2. The changing relationship between summer insolation and the 2015GP record

When placed in time, the comparisons between June insolation at 40°N (Fig. 5A) and the 2015GP records (Fig. 5B–E) show more clearly the precessional-scale variation in climate in the NwTP from late marine isotope stage (MIS) 3 to the end of MIS2. The comparisons between the trends of insolation and 2015GP records during the glacial suggest warm and wet MIS3 conditions, characterized by high insolation, $\delta^{18}O$, and NH_4^+ concentrations (Fig. 5A, B, C) and low dust concentrations (Fig. 5D), that are consistent with the expansion of wetlands and lakes in the NwTP and the Tarim Basin north of Guliya (Herzschuh, 2006; Yang et al., 2006, 2011; Liu et al., 2019). High-d-excess values during MIS3 (Fig. 5E) indicate that local and regional recycled moisture comprised much of the precipitation. As summer insolation decreased from MIS3 to MIS2, the northern TP climate transitioned to colder and drier conditions as demonstrated by lower $\delta^{18}O$ and NH_4^+ and higher dust concentrations. This is consistent with geomorphological and lacustrine paleoclimate records from the northern TP (Herzschuh, 2006; Yang et al., 2011; Zhang et al., 2016; Zhou et al., 2022) and with model-data comparisons (Yu et al., 2007). The diminishing local and regional moisture sources resulted in less evaporation and moisture recycling, which resulted in lower d-excess values in precipitation during MIS2.

Not only do $\delta^{18}O$, NH_4^+, and dust concentration demonstrate orbital-scale variations either in phase or in antiphase with insolation during MIS2 and MIS3, these parameters (along with d-excess) are significantly correlated with each other at the 99.99% level (Table 2), demonstrating consistent climatic variations (wet/warm vs. cold/dry). The exception is the correlation coefficient ($R = +0.05$) between $\delta^{18}O$ and dust concentration from 0 to 17.5 ka BP.

In contrast, the relationships between the 2015GP parameters and summer insolation do not persist after ~17.5 ka BP, or shortly after the end of the Last Glacial Maximum (LGM) in the Northern Hemisphere as determined by Clark et al. (2009). Although Guliya $\delta^{18}O$ varies with summer insolation until the LGM, the trend flattens during the

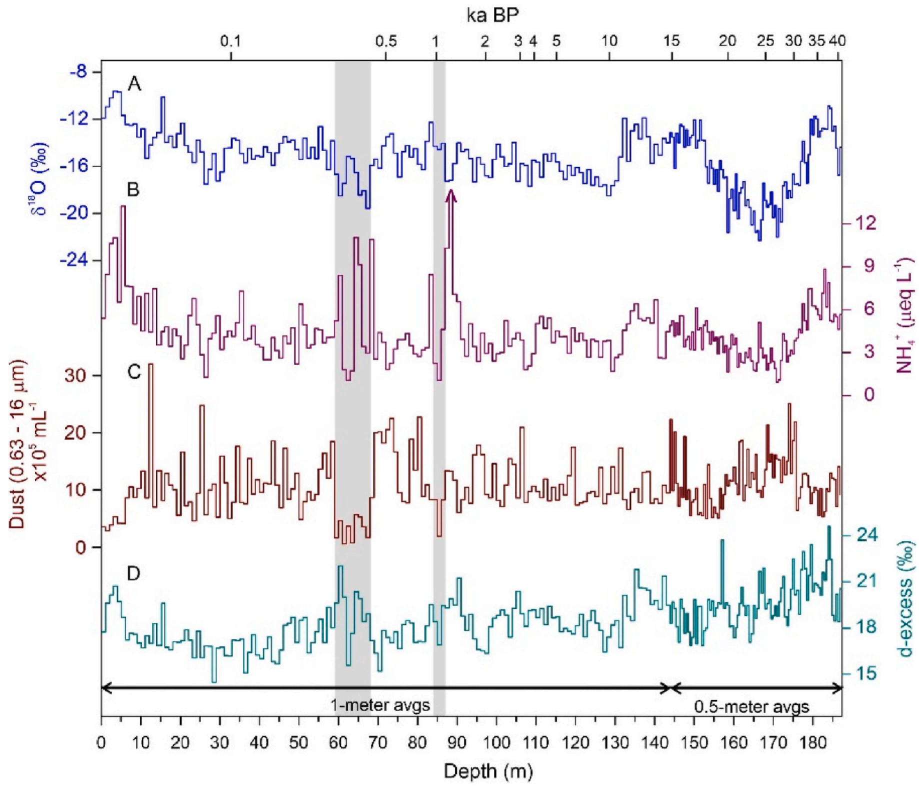

Fig. 4. 2015GP parameters in depth. Physical and chemical data from 2015GP discussed in text, presented by depth with ages shown along top x-axis: (A) $\delta^{18}O$, (B) ammonium (NH_4^+), (C) dust concentration, and (D) d-excess. Gray bars indicate intervals in the cores where the stratigraphy is anomalous, possibly due to crevasse fill. The upward oriented arrow in (B) at ~89 m indicates an NH_4^- concentration (16.36 μeq L^{-1}) that exceeds the upper limit of the y-axis value.

deglaciation period (~17.5–~12 ka BP) as the insolation curve continues to rise. The trends between $\delta^{18}O$ and insolation are opposite throughout the Holocene, suggesting that the influences on isotopic fractionation may have changed (Fig. 5A and B).

Although the effects of insolation on NwTP may have changed between the glacial and the Holocene, the relationships between the 2015GP parameters remained significant and consistent except for $\delta^{18}O$ and dust concentration (Table 2). In order to determine whether these relationships are dominated by precessional variations, the same calculations are performed on the detrended 2015GP records during the pre- and post-LGM periods (Supplement Table S2.1). The post-LGM (0–17.5 ka BP) R values of the detrended time series are close to those in Table 2, while the R values of the glacial stage correlations are less significant. These changing relationships between mid-latitude summer insolation and NwTP climate, along with the changing relationships between temperature, humidity/aridity, and moisture pathways as observed in the Guliya record, suggest that this region of the TP was sensitive to changing hemisphere-wide boundary conditions as Earth emerged from the last glacial stage.

3.3. *The Guliya Holocene $\delta^{18}O$ conundrum*

According to the interpretation of the 2015GP parameters discussed in Section 3.1.1, the Guliya record implies that the warm and wet climate in the NwTP during the deglaciation abruptly switched to cold and arid conditions as the Holocene began and gradually transitioned to a warmer and wetter climate toward the present despite the antiphase relationship with insolation (Fig. 5). However, a synthesis of paleoclimate records based on temperature proxies from the TP (Zhang et al., 2022a) reveals that summer temperature increased with summer insolation during the late deglaciation into the Early Holocene. As the Holocene progressed both summer temperature and insolation decreased, while winter and annual temperatures increased (Zhang et al., 2022a). The Holocene 2015GP $\delta^{18}O$ record demonstrates a similar trend to a reconstructed temperature stack for low latitudes (30°N to 30°S) (Marcott et al., 2013) until they diverge around 3.5 ka BP. However, the 2015GP $\delta^{18}O$ record deviates from the higher latitude (30°N to 70°N) Northern Hemisphere reconstructed temperature stack (Marcott et al., 2013), which like summer insolation shows a decreasing trend through the Holocene.

Here we discuss possible scenarios to explain the diverging trends between summer insolation and 2015GP $\delta^{18}O$ (Fig. 6A and B). One explanation is that the seasonality of precipitation in the NwTP gradually shifted from summer to winter during the deglaciation and remained so until the Late Holocene. Although this scenario would bring 2015GP $\delta^{18}O$ in alignment with mid-latitude winter insolation and high latitude temperature trends (Marcott et al., 2013), it is contradicted by Cai et al. (2017) who concluded from speleothem $\delta^{18}O$ analysis that changes in precipitation seasonality did not occur during the Holocene in western China.

A second scenario is based upon the assumption that $\delta^{18}O$ in Guliya ice continued to record temperature after the deglaciation; however, the primary climate forcing was rising concentrations of greenhouse gases (Fig. 6C) Liu et al., 2014. In fact, the upward trend in 2015GP $\delta^{18}O$ since the Middle Holocene (~8 ka BP) (Fig. 6B) is similar to CO_2 concentrations from Dome C, Antarctica (Monnin et al., 2004) (Fig. 6C), implying that temperature in this high-elevation region was controlled by radiative forcing rather than insolation during this period. However, this does not explain why 2015GP $\delta^{18}O$ decreased abruptly at the beginning of the Holocene as CO_2 abruptly increased.

A third possible explanation for the 2015GP $\delta^{18}O$ deglaciation and Holocene record precludes temperature as a primary influence and instead assigns moisture source and pathways as the most important factors in isotopic fractionation in precipitation. This scenario, which is discussed in more detail below, is dependent on variations in the intensity and position of major air masses over the NwTP as well as

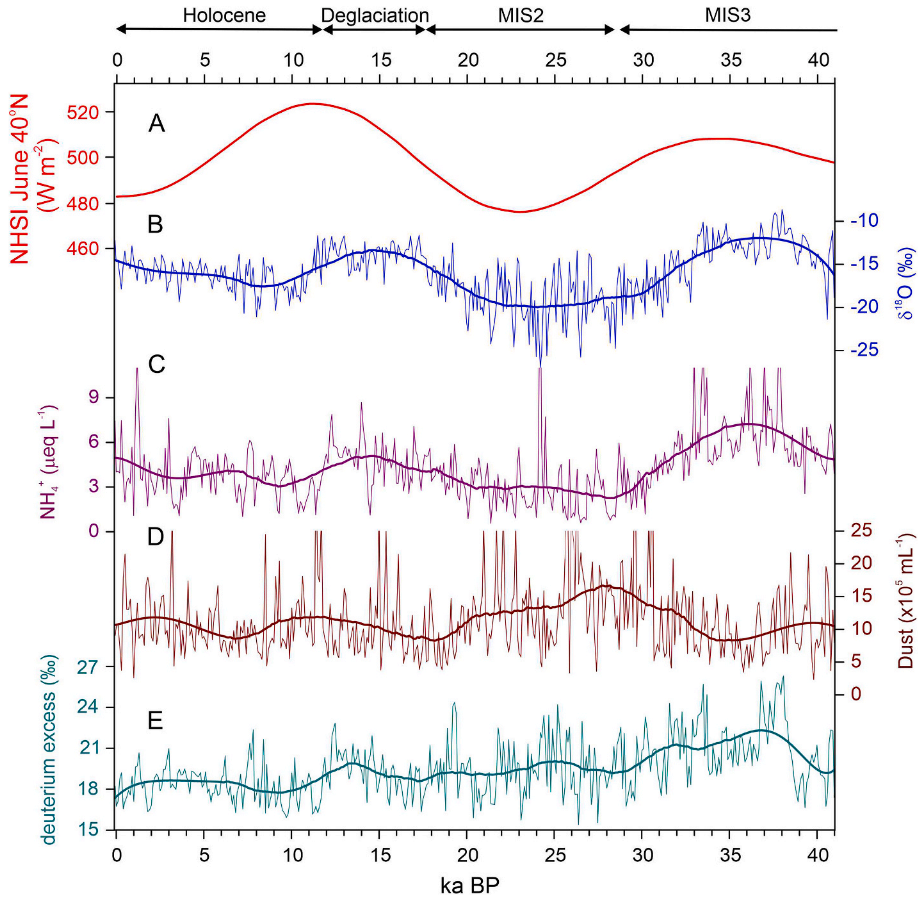

Fig. 5. Guliya records compared with summer insolation. (A) June insolation at 40°N (Berger and Loutre, 1991) is compared with the 2015GP records of (B) $\delta^{18}O$, (C) NH_4^+, (D) dust concentrations, and (E) deuterium excess. The Guliya records are presented as 100-year averages overlain by LOESS smoothing curves (5th degree polynomial, sampling proportion = 0.3).

Table 2

Correlation coefficients (R) between 2015GP parameters. The 41 kyr records are divided into two intervals: 0 to 17.5 ka BP (Holocene and deglaciation) and 17.5 to 41 ka BP (MIS2 and Late MIS3). All the time series were smoothed with five-century running means. Values in bold red are significantly negative R values ($p < 0.001$), in bold black are significantly positive R values ($p < 0.001$).

Guliya plateau core		NH_4^+	Dust concentration	d-excess
$\delta^{18}O$	0 – 17.5 ka BP	**+0.50**	+0.05	**+0.43**
	17.5 – 41 ka BP	**+0.79**	**-0.41**	**+0.56**
NH_4^+	0 – 17.5 ka BP		**-0.36**	**+0.55**
	17.5 – 41 ka BP		**-0.56**	**+0.62**
Dust concentration	0 – 17.5 ka BP			**-0.27**
	17.5 – 41 ka BP			**-0.24**

boundary conditions, such as Northern Hemisphere ice sheet size, which decreased rapidly during the Early Holocene (Fig. 6D).

Finally, the sudden decrease of 2015GP $\delta^{18}O$ at the beginning of the Holocene may have involved the temperature of the local and regional precipitation sources. Summer insolation warmth spurred glacier melting, both on the TP and in the high latitudes of Eurasia. Maximum glacier meltwater into Guozha Co to the south of the west Kunlun ice sheet occurred ~9.5 to 8.5 ka BP (Li et al., 2021). The influx of cold, ^{18}O-depleted meltwater into local lakes provided a source of lower $\delta^{18}O$ precipitation for the glaciers in the NwTP. Several studies on lakes in the western TP during the Holocene found that levels were high in the Early Holocene, although some conclude that this was a consequence of higher precipitation from the northward moving monsoon (Herzschuh, 2006; Hudson and Quade, 2013; Hou et al., 2017).

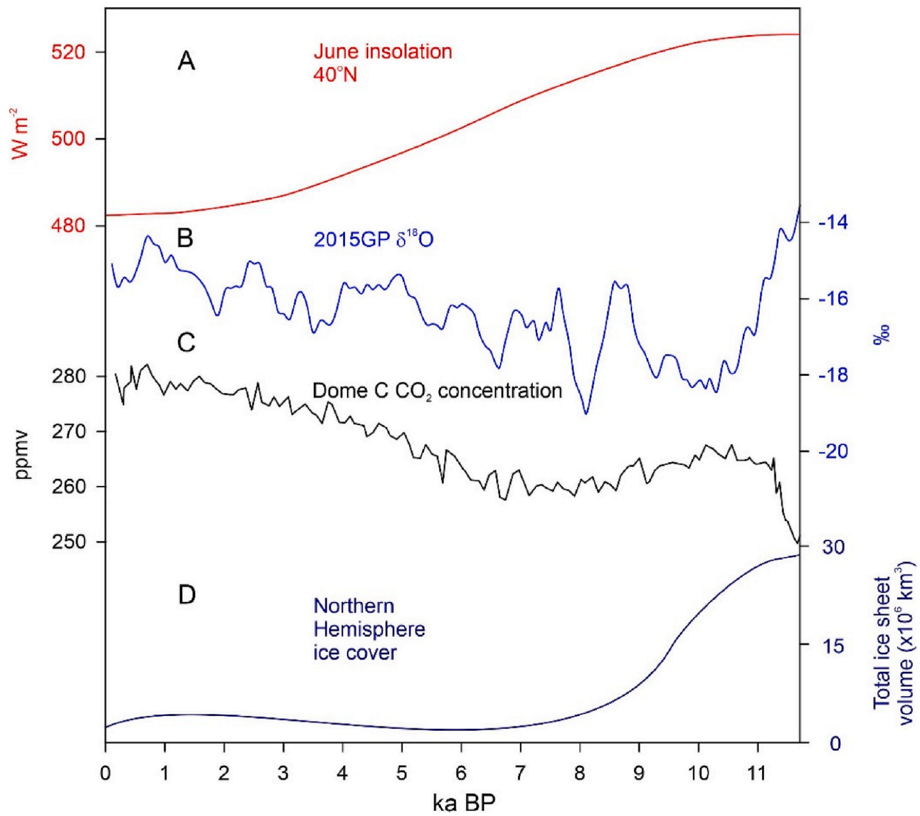

Fig. 6. Climate forcings during the Holocene (since 11.7 ka BP). (A) Summer (June) insolation at 40°N (Berger and Loutre, 1991) is compared with (B) δ^{18}O from 2015GP (5-century running means), (C) CO_2 concentrations from Dome C, East Antarctica (Monnin et al., 2004), and (D) modeled Northern Hemisphere ice volume (Zweck and Huybrechts, 2005). The Antarctic CO_2 data are from https://www.ncei.noaa.gov/pub/data/paleo/icecore/antarctica/epica_domec/edc3-composite-co2-2008-noaa.txt.

3.4. Comparison of Guliya 2015GP record with North Atlantic and tropical Asian climate records

During late MIS3 through MIS2 the total volume of the Northern Hemisphere ice cover steadily grew to a maximum at ~18 to 19 ka BP, followed by a rapid decrease as summer insolation increased through the deglaciation (~17–~12 ka BP) (Fig. 7A). The Greenland GISP2 ice core δ^{18}O record, a proxy for temperature in the North Atlantic (Mayewski and Bender, 1995) (Fig. 7B) generally is out of phase with the trend of the ice volume changes since late MIS3, while ice volume changes are in phase with the speleothem δ^{18}O record of ISM intensity from Mawmluh Cave in northeastern India (Dutt et al., 2015) (Fig. 7C). The Greenland ice core and ISM δ^{18}O records are negatively correlated at significant levels (−0.81, $p < 0.001$, 100-yr averages) over the last 41 kyr, which is consistent with the well-established link between North Atlantic temperature and migration of the monsoons and intensification or weakening of precipitation in the Indian monsoon region (Burns et al., 2003; Gupta et al., 2003; Goswami et al., 2006; Feng and Hu, 2008; Deplazes et al., 2013; Marzin et al., 2013; Tierney et al., 2016; Jaglan et al., 2021).

On the precessional timescale the warm and wet conditions during late MIS3 and the cold and dry MIS2 climate on the NwTP, as depicted by 2015GP δ^{18}O, NH_4^+, and dust concentrations (Fig. 7D–F), show similarities with North Atlantic climate (GISP2 δ^{18}O). The reversal in trends between summer insolation and the 2015GP δ^{18}O, NH_4^+, and dust records through the deglaciation to the Holocene (Fig. 5; Fig. 7A, D-F) is also observed in the correlation coefficients between the Guliya stable isotope and NH_4^+ records and the GISP2 and Mawmluh Cave δ^{18}O records, which reverse sign from their pre-deglaciation to post-LGM values (Table 3). As in Table 2, the dust concentration R values are the exception to these relationships, showing significant correlation (−0.20, $p < 0.01$) with GISP2 δ^{18}O only during the glacial.

Heinrich Events 2, 3, and 4 are visible in 2015GP and GISP2 δ^{18}O and d-excess as isotopic depletions (Fig. 7B, D, G), although there is no consistent expression of the events in the other Guliya parameters. Millennial-scale events during the deglaciation that are obvious in the GISP2 and speleothem δ^{18}O records, such as Heinrich Event 1 (H1), the Bølling/Allerød (B/A) and the Younger Dryas (YD) (Fig. 7B and C), also appear in 2015GP δ^{18}O (Figs. 7D, Fig. 8A–C). These events in the GISP2 and Indian cave records show consistently opposite δ^{18}O trends throughout the 41 kyr record. However, like the orbital-scale variations discussed above, the relationships of these millennial-scale events in the tropical and polar records with 2015GP δ^{18}O reverse after the onset of the deglaciation (Fig. 8A–C) such that H1 and YD are characterized by ^{18}O enrichment and the B/A by ^{18}O depletion. The Guliya records paradoxically suggest climate forcings during these events that differ from those deduced from other Tibetan Plateau climate records (i.e., cold H1 and YD, warm B/A) (Gasse et al., 1991; Chen et al., 1997; Zhu et al., 2015).

4. Discussion

The orbital-scale similarities between summer insolation (Fig. 7A), which increased sensible heating on the TP, and 2015GP δ^{18}O (Fig. 7D) during MIS3 and MIS2 indicate that the isotopic fractionation in Guliya precipitation was largely controlled by summer temperature. The volume of the Northern Hemisphere ice cover increased through MIS2 (Fig. 7A), forcing the midlatitude westerly jet southward as the previous warm/wet climate transitioned to cold and arid conditions. Millennial-scale events in the ice core which vary in phase with those in the Greenland ice core (Fig. 7B) confirm observations that the changes in the Atlantic meridional overturning circulation and temperature variations in the North Atlantic were transported to the NwTP by the westerlies

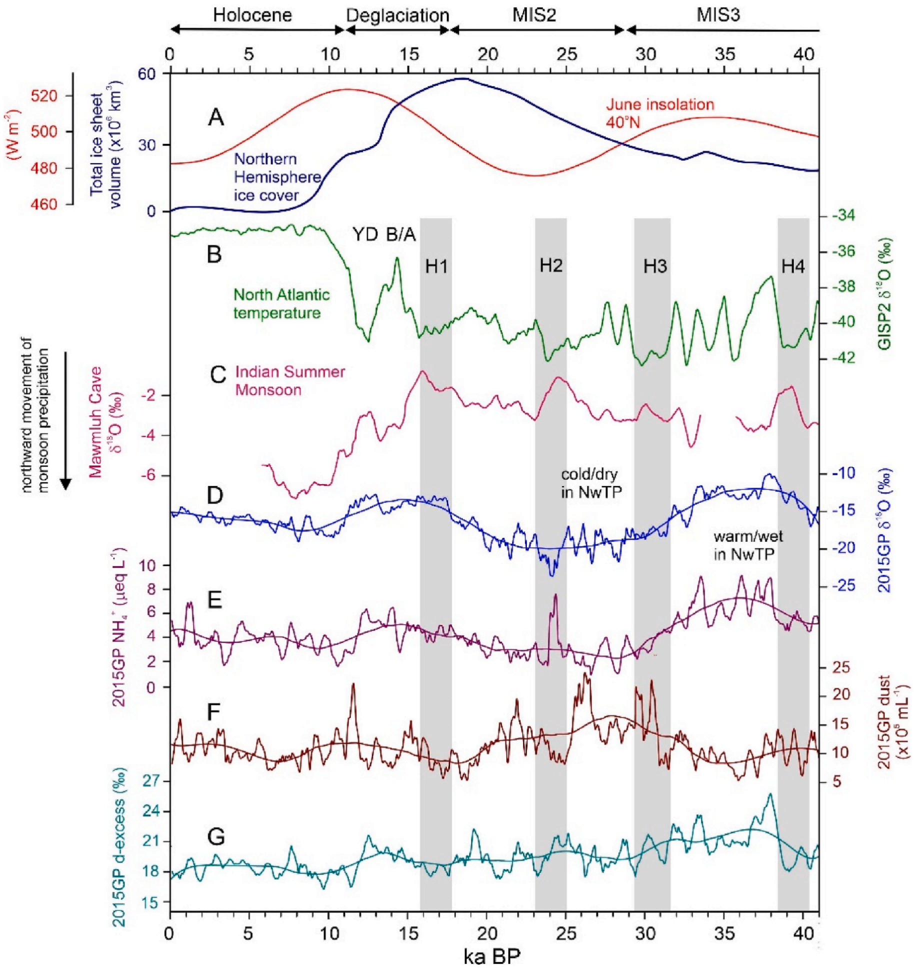

Fig. 7. Comparisons of polar and tropical records to Guliya records since the late MIS3. (A) Northern Hemisphere spring insolation at 40°N (red curve, Berger and Loutre, 1991) and total Northern Hemisphere ice volume (blue curve, Zweck and Huybrechts, 2005); (B) the $\delta^{18}O$ record from the GISP2 ice core (Grootes and Stuvier, 1997) and (C) the $\delta^{18}O$ record of Indian summer monsoon intensity from Mawmluh Cave, NE India (Dutt et al., 2015) are compared with Guliya records of (D) $\delta^{18}O$, (E) NH_4^+, (F) dust concentrations, and (G) deuterium excess. The GISP2 and Mawmluh $\delta^{18}O$ records and all Guliya profiles are presented as 5-century moving averages, and the Guliya records are overlain by LOESS smoothing of 100-year averages (5th order polynomial, sampling proportion = 0.3). Heinrich Events H1 to H4 are marked by gray bars.

Table 3
Correlation coefficients (R) between 2015GP parameters and GISP2 and Mawmluh Cave $\delta^{18}O$ time series. The 41 kyr records are divided into two intervals: 0 to 17.5 ka BP (Holocene and deglaciation) and 17.5 to 41 ka BP (MIS2 and Late MIS3). All the time series were smoothed with five-century running means. Values in bold red are significantly negative R values ($p < 0.001$), in bold black are significantly positive R values ($p < 0.001$), and the R between 2015GP dust and GISP2 $\delta^{18}O$ is significant at $p < 0.01$. All other R values are not significantly correlated.

		2015GP $\delta^{18}O$	2015GP NH_4^+	2015GP Dust	2015GP d-excess
GISP2 $\delta^{18}O$	0 – 17.5 ka BP	**-0.81**	**-0.38**	+0.01	**-0.36**
	17.5 – 41 ka BP	**+0.41**	**+0.35**	-0.20	**+0.43**
Mawmluh Cave $\delta^{18}O$	0 – 17.5 ka BP	**+0.86**	**+0.44**	+0.03	**+0.31**
	17.5 – 41 ka BP	**-0.31**	**-0.33**	+0.03	**-0.31**

during the last glacial (Li et al., 2016). Cold Heinrich Events in the glacial stage of the GISP2 and 2015GP ice core records align with high $\delta^{18}O$ in the ISM speleothem record (Fig. 7C) which resulted from southward monsoon migration and weakening of monsoon intensity in South Asia. These orbital and suborbital variations in the glacial stage climate in the NwTP apparently are linked to the cryosphere and to the atmospheric and oceanic temperatures and circulations in the North Atlantic, to the mid-latitude westerlies that originate in the North Atlantic, and potentially to the position of the monsoon.

The deglaciation and Holocene $\delta^{18}O$ records from GISP2, 2015GP, and the Mawmluh and Qunf Cave (Oman) speleothems from the ISM region (Fig. 8A–C) show in greater detail the stronger in-phase similarities between the NwTP climate and the ISM and the anti-phase relationship with North Atlantic air temperature. The reversal in

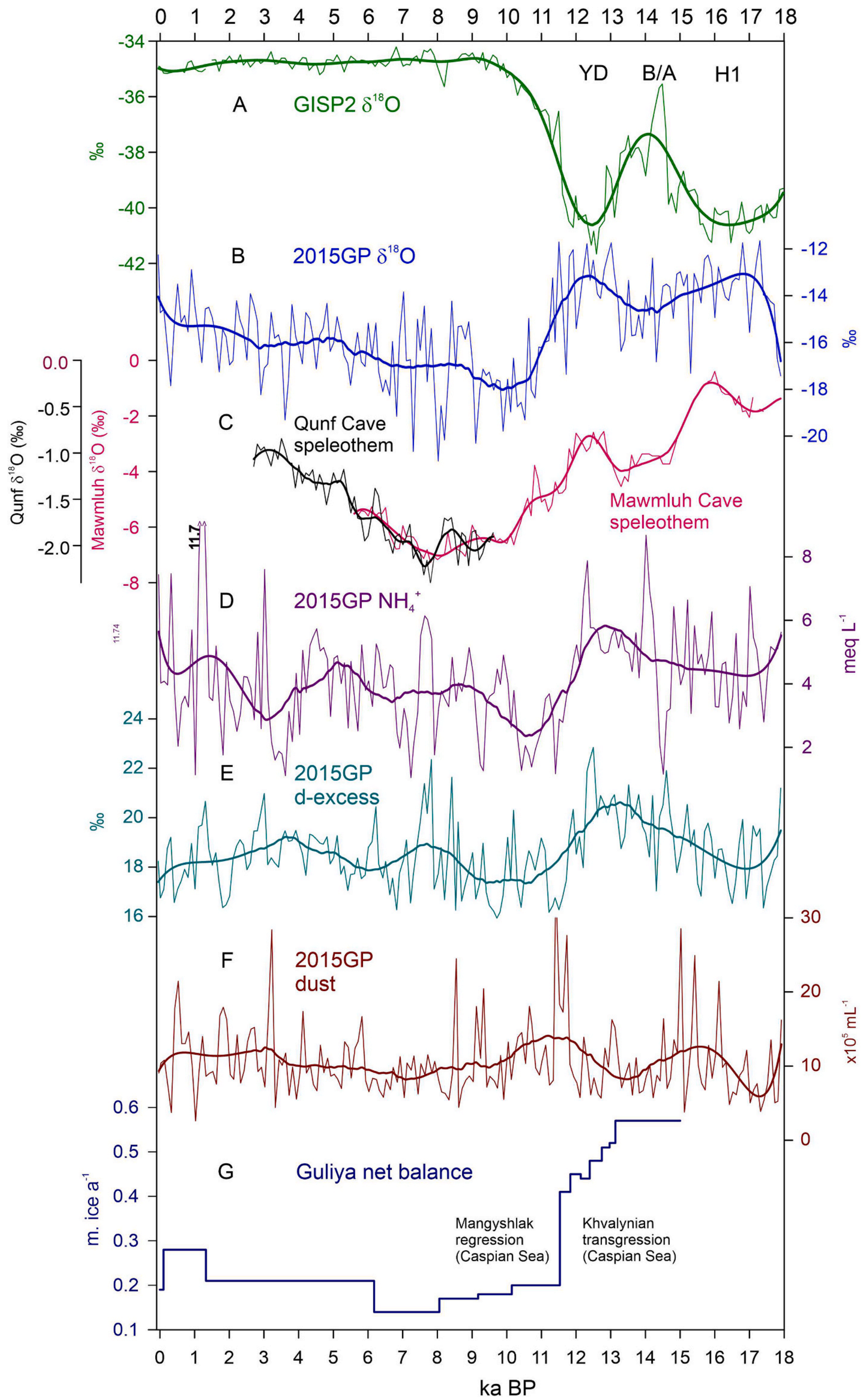

Fig. 8. Climatic variations in the NWTP since the LGM. Centennial averages (thin lines) overlain by LOESS-smoothed curves (thick lines; 5th order polynomial, sampling proportion = 0.3) of (A) GISP2 $\delta^{18}O$ (Grootes and Stuvier, 1997), (B) 2015GP $\delta^{18}O$, (C) speleothem $\delta^{18}O$ from Qunf Cave, Oman (Fleitmann et al., 2003) and Mawmluh Cave, NE India (Dutt et al., 2015), (D) 2015GP NH_4^+, (E) 2015GP d-excess, and (F) 2015GP dust concentrations are compared with (G) the net balance record reconstructed from a Guliya summit core showing the Caspian Sea regression and transgression phases (Koriche et al., 2022).

correlations between the climate record from Guliya and the GISP2 and speleothem records shortly after the onset of the deglaciation implies that the retreat of the thick continental ice cover was linked to the decreasing influence of high latitude forcing via westerlies on both millennial and orbital timescales. As the summer insolation peaked at the beginning of the Holocene and the ISM moved northward with the Atlantic ITCZ (Arbuszewski et al., 2013), the Guliya stable isotope values and NH_4^+ decreased (Fig. 8B, D, E) as dust concentration increased (Fig. 8F) contemporaneously with $\delta^{18}O$ increase in GISP2 (Fig. 8A), despite indications of Early Holocene insolation-driven warming and an increasingly wet climate from regional proxy climate records (Gasse et al., 1991; Herzschuh, 2006; Zhang et al., 2022b). This change in climatic influence around this time is not unique to Guliya, as it is also present in a pollen record from a lacustrine core from Nam Co (Fig. 1A)

(Zhu et al., 2015), located ~1000 km to the southeast of Guliya and closer to the monsoon precipitation source. In the Nam Co record this transition was explained as a change in the dominant atmospheric circulation from westerlies to monsoonal resulting from the northward migration of the westerlies and the ISM. Meanwhile, the isotopic enrichment in the 2015GP core during H1 and the YD and the depletion during the B/A warming, opposite to the GISP2 record, suggests a weakening of the climate connection between the North Atlantic and the NwTP. Increasing summer insolation quite likely remained an important forcing of temperature and moisture during the deglaciation, although some combination of conditions occurred beginning in the deglaciation that led to the divergence of the 2015GP $\delta^{18}O$ and summer insolation and the change in correlations between Guliya and the North Atlantic and tropical climate records (Table 3).

4.1. Possible explanations for the glacial/post glacial isotopic switch in 2015GP

There are two possible explanations for the switch in the relationship between the Guliya and the other proxy records that occurred as the glacial stage ended: (1) tropical moisture sources may have indirectly contributed to the isotopic composition of the NwTP precipitation as the westerlies and ISM moved northward, or (2) changes in both isotopic fractionation in precipitation and in aerosol concentrations resulted from atmospheric and environmental alterations in the NwTP and Central Asia as the Northern Hemisphere emerged from the last glacial stage.

4.1.1. Increasing monsoon moisture influx after the last glacial maximum

The first explanation assumes that monsoon moisture was able to extend to the western Kunlun Mountains. Extreme monsoon low-pressure systems can produce precipitation on the Tibetan Plateau that contains moisture which is characterized by lower d-excess (Bershaw, 2018). Using observational data and model simulations, Dong et al. (2016, 2017) discuss an "up and over" mechanism of ISM moisture onto the TP through the uplift of northward moving convective storms over the Himalayas. According to Dong et al. (2016) half of the total summer precipitation in the southwestern TP is derived from this pathway. By the latitude of Guliya (35°N) much of this effect would dissipate but as most of the summer precipitation in the western Kunluns is from moisture recycling (An et al., 2017), some of the summer snow that falls on the ice cap may be recycled monsoon moisture from the south. Mid-tropospheric circulation maps (Dong et al., 2017) indicate that winds are southerly during monsoon low-pressure events which would result in monsoon-derived moisture being recirculated northward. Isotope modeling by An et al. (2017) demonstrates that low d-excess in precipitation on the nearby Chongce glacier may result from monsoon contribution to the summer snowfall. If recycled moisture from the ISM reaches the NwTP today, then it should have reached that far north during the onset of the Holocene when summer insolation was at its peak and the ISM approached its northernmost extent and greatest intensity in South Asia as demonstrated by very low $\delta^{18}O$ in ISM speleothem records (Figs. 7C and 8C). The actual northward extent of ISM precipitation during this period is uncertain, with some investigators concluding that it reached the southern and southeastern TP (Bird et al., 2014; Zhu et al., 2015) and even as far north as the Kunlun Mountains (Ramisch et al., 2016) and arid Central Asia (Cheng et al., 2012).

Both the 2015GP $\delta^{18}O$ and d-excess decreased contemporaneously with the ISM speleothem $\delta^{18}O$ at the beginning of the Holocene (Fig. 8B, C, E). According to isotope modeling results (An et al., 2017) this implies that there were periods of increased influx of some recycled monsoon moisture to the Guliya ice cap. The centennial averages of 2015GP d-excess show that this was not a constant monsoon contribution; rather, there were several short periods of low d-excess that may have corresponded to intense low-pressure monsoon activity.

4.1.2. Variations in intensity of the westerlies

The effects of the westerlies and availability of moisture on Guliya $\delta^{18}O$, NH_4^+ and d-excess during the glacial may have continued through the deglaciation and Holocene, with moisture recycling from lakes and wetlands in the NwTP and Central Asia being the primary influence on the stable isotopes, particularly d-excess. A 15 kyr net balance record (Fig. 8G) reconstructed from one of the cores drilled on the GS (Supplement Section S3) shows high snow accumulation on the ice cap during the B/A (~13–15 ka BP) when enriched isotopes in GISP2 (Fig. 8A) were contemporaneous with increasing summer insolation. At the same time overall levels of 2015GP $\delta^{18}O$, NH_4^+, and d-excess (Fig. 8B, D-E) were high while dust concentrations decreased (Fig. 8F), although the B/A in 2015GP $\delta^{18}O$ is marked by ^{18}O depletion and is less prominent than in the Greenland record. Although Mawmluh Cave $\delta^{18}O$ indicates that the position of the ISM oscillated during the deglaciation (southward during H1 and the YD, northward during the B/A) (Fig. 8C), the source of the precipitation on Guliya at this time was likely local and regional recycled moisture may have been augmented by recycled moisture from large water bodies in Central Asia. For example, during the B/A when Guliya net balance was high the Caspian Sea expanded during the "Khvalynian transgression" (Fig. 8G) as discharge from glacial streams originating from the melting Eurasian ice cover increased (Koriche et al., 2022). Model studies suggest that changes in the surface area of the Caspian Sea may have profound effects on climate to the east and may extend to the northern Pacific Ocean (Koriche et al., 2021).

Both the Guliya NH_4^+ concentration and net balance decreased as the YD ended and the Holocene began (Fig. 8D, G), which implies fewer available water sources both locally and to the west. This is supported by the opposing trend in the dust concentrations in the YD and Early Holocene (Fig. 8F). This apparent decreasing trend in precipitation on the Guliya ice cap through the Early Holocene contrasts with increasing effective moisture reconstructed from lake levels and lacustrine core analyses throughout the western and central TP (Gasse et al., 1991; Herzschuh, 2006; Hudson and Quade, 2013). One possible explanation for this discrepancy is that higher insolation-driven summer temperatures (Li et al., 2021) increased ablation on glaciers on the TP, resulting in reduced net ice accumulation. Consequently, the resulting glacial meltwater raised lake levels in the region. However, the abrupt net balance decline in the 2015GP core at the beginning of the Early Holocene (Fig. 8G) agrees with the regressive phase of the Caspian Sea ("Mangyshlak regression") which may have deprived Guliya of an important source of moisture. Routson et al. (2019) found that a weaker latitudinal temperature gradient during the Early Holocene resulted in diminished westerlies and lower mid-latitude net precipitation, which would have reduced moisture evaporation and recycled precipitation to the ice cap. This scenario is illustrated in the 2015GP core as low $\delta^{18}O$, NH_4^+ concentrations and d-excess (Fig. 8B, D, E) and high dust concentrations (Fig. 8F).

From the Middle Holocene to the present, the Guliya $\delta^{18}O$, NH_4^+, and net balance gradually increased (Fig. 8B, D, G) as the ISM retreated southward, although NH_4^+ shows more millennial-scale variability. The increasing mid-latitude temperature gradient since ~8 ka BP, linked to decreasing summer insolation, generated more frequent mid-latitude cyclogenesis (Routson et al., 2019). The trends displayed by the Guliya net balance and NH_4^+ records indicate that the western Kunlun Mountains may have received its precipitation from local moisture recycling and from the westerlies that migrated southward following the ITCZ (Arbuszewski et al., 2013).

5. Conclusions

The ice core drilled from the plateau of the Guliya ice cap provides a long, unique record of climate variations in the Northwest Tibetan Plateau. The $\delta^{18}O$, d-excess, NH_4^+, and dust concentrations time series reveal how the climate in this region is affected on multiple timescales by changes in the intensity of the mid-latitude westerlies originating in the North Atlantic and possibly by the migration of the Indian summer monsoon during the deglaciation and Holocene. The variations in these influences are controlled by Northern Hemisphere ice sheet extent, the movement of the ITCZ, and insolation. The $\delta^{18}O$, NH_4^+, and dust concentration records, which show warm and wet conditions during MIS3 and cold and dry conditions during MIS2, indicate that during the glacial stage the climate in the NwTP was forced on orbital timescales by insolation and Northern Hemisphere ice sheet extent. However, on millennial timescales the Guliya records correspond positively with North Atlantic temperatures, supporting research that cold episodes such as the Heinrich Events were linked to climate conditions in the North Atlantic that were transferred eastward by the westerlies (Li et al., 2016). Compared with the relatively straightforward linkages among summer insolation, polar air masses, and the climate in the NwTP during MIS2 and MIS3, the Guliya deglaciation records demonstrate influences on the NwTP that are governed by higher summer insolation and rapidly retreating Northern Hemisphere ice cover. During the deglaciation increasing summer insolation still influenced the temperature in the region, but millennial-scale features such as the Heinrich Event 1, the Bølling/Allerød, and the Younger Dryas were anti-phase (in-phase) with the North Atlantic temperature (monsoon intensity), the reverse of the relationships during the glacial. These shifting relationships suggest that as the glacial stage ended and the deglaciation began moisture delivered by the westerlies waned. By the Early Holocene some recycled ISM moisture may have reached the NwTP, although not enough to compensate for the loss of moisture from Central Asian lakes and local sources. Alternatively, the stable isotope variations in the Guliya record may have been controlled primarily by variations in the position and intensity of the mid-latitude westerlies and the availability of recycled moisture. The post-glacial reversal in the correlation between summer insolation and 2015GP $\delta^{18}O$, which is most pronounced during the Holocene, may indicate either changing influences on isotopic fractionation or the effects of changing boundary conditions on the climate and environment in the NwTP and Central Asia as recorded in the Guliya ice core. The upward trend in $\delta^{18}O$ during the Holocene may in part reflect warming on the Tibetan Plateau which was forced by rising greenhouse gas concentrations. Further investigation is required to understand: (1) the atmospheric and hydrospheric processes governing the fractionation of stable isotopes of water in the NwTP, and (2) the transient relationships between the boundary conditions and the climate of this region that is located close to a migrating border between competing air masses.

Credit author statement

All the authors made substantial contributions to this submission. L. G. Thompson and E. Mosley-Thompson are the Principal Investigators on the Guliya project. L. G. Thompson and T.-D. Yao co-led the field work, and G. Wu and S. Kutuzov participated in the field work. H.-A. Synal and J. Beer provided cosmogenic isotope data. J. F. Bolzan reconstructed the net balance record. E. B. and M. R. S.-H. prepared samples for processing. M. E. Davis organized and archived the ice core data. All the authors contributed to data interpretation and manuscript preparation and approved the revised version.

Declaration of competing interest

The authors declare that they have no known competing financial interests or personal relationships that could have appeared to influence the work reported in this paper.

Data availability

I have shared the link to the data at teh Attach File step

Guliya Ice Cap, China, -0.064 41ka BP stable isotope, NH4, dust data (Original data) (NCEI)

Acknowledgements

This work was supported by the National Science Foundation Paleo Perspectives on Climate Change Program [Award 1502919]. The authors want to thank Ping-Nan Lin for stable isotope analysis, Donald Kenny for dust and major ion analysis, and Anita Schlatter (EAWAG) for the ^{10}Be and ^{36}Cl analyses. We thank all the field team members from the Byrd Polar and Climate Research Center and the Institute for Tibetan Plateau Research. The authors also want to thank two reviewers for their critiques and suggestions that helped improve this paper. This is Byrd Polar and Climate Research Center Contribution Number C-1626.

Appendix A. Supplementary data

Supplementary data to this article can be found online at https://doi.org/10.1016/j.quascirev.2023.108443.

References

Aggarwal, P.K., Romatschke, U., Araguas-Araguas, L., Belachew, D., Longstaffe, F.J., Berg, P., Schumacher, C., Funk, A, 2016. Proportions of convective and stratiform precipitation revealed in water isotope ratios. Nat. Geosci. 9, 624–629. https://doi.org/10.1038/NGEO2739.

An, W., Hou, S., Zhang, Q., Zhang, W., Wu, S., Xu, H., Pang, H., Wang, Y., Liu, Y., 2017. Enhanced recent local moisture recycling on the northwestern Tibetan Plateau deduced from ice core deuterium excess records. J. Geophys. Res. Atmos. 122 (12), 12,541–12,556. https://doi.org/10.1002/2017JD027235.

An, W., Hou, S., Zhang, W., Wu, S., Xu, H., Pang, H., Wang, Y., Liu, Y., 2016. Possible recent warming hiatus on the northwestern Tibetan Plateau derived from ice core records. Sci. Rep. 6, 32813. https://doi.org/10.1038/srep32813.

An, Z., Sun, Y., Zhou, W. Liu, W., Qiang, X., Wang, X., Xian, F., Cheng, P., Burr, G. S., 2014. Chinese loess and the East Asian monsoon. In: An, Z. (Ed.), Late Cenozoic Climate Change in Asia. Springer, Dordrecht, pp. 23–144.

Aneja, V.P., Roelle, P.A., Murray, G.C., Southerland, J., Erisman, J.W., Fowler, D., Asman, W.A.H., Patni, N., 2001. Atmospheric nitrogen compounds II: emissions, transport, transformation, deposition and assessment. Atmos. Environ. 35, 1903–1911. https://doi.org/10.1016/S1352-2310(00)00543-4.

Arbuszewski, J.A., deMenocal, P.B., Cléroux, C., Bradtmiller, L., Mix, A., 2013. Meridional shifts of the Atlantic intertropical convergence zone since the Last Glacial Maximum. Nat. Geosci. 6, 959–962. https://doi.org/10.1038/ngeo1961.

Beer, J., McCracken, K., von Steiger, R., 2012. Cosmogenic Radionuclides: Theory and Applications in the Terrestrial and Space Environments. Springer, Berlin.

Belmaker, R., Stein, M., Beer, J., Christl, M., Fink, D., Lazar, B., 2014. Beryllium isotopes as tracers of Lake Lisan (last glacial Dead Sea) hydrology and the Laschamp geomagnetic excursion. Earth Planet Sci. Lett. 400, 233–242. https://doi.org/10.1016/j.epsl.2014.05.049.

Benson, L., Liddicoat, J., Smoot, J., Sarna-Wojcicki, A., Negrini, R., Lund, S., 2003. Age of the Mono Lake excursion and associated tephra. Quat. Sci. Rev. 22, 135–140. https://doi.org/10.1016/S0277-3791(02)00249-4.

Berger, A., Loutre, M.F., 1991. Insolation values for the climate of the last 10 million years. Quat. Sci. Rev. 10, 297–317. https://doi.org/10.1016/0277-3791(91)90033-Q.

Bershaw, J., 2018. Controls on deuterium excess across Asia. Geosciences 8, 257. https://doi.org/10.3390/geosciences8070257.

Bird, B.W., Polisar, P.J., Lei, Y., Thompson, L.G., Yao, T., Finney, B.P., Bain, D.J., Pompeani, D.P., Steinman, B.A., 2014. A Tibetan lake sediment record of Holocene Indian summer monsoon variability. Earth Planet Sci. Lett. 299, 92–102. https://doi.org/10.1016/j.epsl.2014.05.017.

Bouwman, A.F., Lee, D.S., Asman, W.A.H., Dentener, F.J., Van Der Hoek, K.W., Olivier, J. G.J., 1997. A global high-resolution emission inventory for ammonia. Global Biogeochem. Cycles 11, 561–587. https://doi.org/10.1029/97GB02266.

Burns, S.J., Fleitmann, D., Matter, A., Kramers, J., Al-Subbary, A.A., 2003. Indian Ocean climate and an absolute chronology over Dansgaard/Oeschger events 9 to 13. Science 288, 847–850. https://doi.org/10.1126/science.1086227.

Cai, Y., Chiang, J.C.H., Breitenbach, S.F.M., Tan, L., Cheng, H., Edwards, R.L., An, Z., 2017. Holocene moisture changes in western China, Central Asia, inferred from stalagmites. Quat. Sci. Rev. 158, 15–28. https://doi.org/10.1016/j.quascirev.2016.12.014.

Cao, B., Guan, W., Li, K., Wen, Z., Han, H., Pan, B., 2020. Area and mass changes of glaciers in the West Kunlun Mountains based on the analysis of multi-temporal remote sensing images and DEMs from 1970 to 2018. Rem. Sens. 12, 2632. https://doi.org/10.3390/rs12162632.

Cassata, W.S., Singer, B.S., Cassidy, J., 2008. Laschamp and Mono Lake geomagnetic excursions recorded in New Zealand. Earth Planet Sci. Lett. 268, 76–88. https://doi.org/10.1016/j.epsl.2008.01.009.

Channell, J.E.T., 2006. Late Brunhes polarity excursions (Mono Lake, Laschamp, Iceland Basin and Pringle Falls) recorded at ODP site 919 (Irminger Basin). Earth Planet Sci. Lett. 244, 378–393. https://doi.org/10.1016/j.epsl.2006.01.021.

Chen, F., Bloemendal, J., Wang, J., Li, J.J., Oldfield, F., 1997. High-resolution multi-proxy climate records from Chinese loess: evidence for rapid climatic changes over the last 75 kyr. Palaeogeogr. Palaeoclimatol. Palaeoecol. 130, 323–335. https://doi.org/10.1016/S0031-0182(96)00149-6.

Chen, J., Li, W., Qiao, P., Li, Y., Zheng, K., Wang, Y., Dong, X., Wang, S., Tan, L., Chu, F., Fang, N., Zeng, Y., 2021. Characterizing ammonia emissions from water bodies using dynamic floating chambers. Sci. Total Environ. 796, 148978. https://doi.org/10.1016/j.scitotenv.2021.148978.

Cheng, H., Edwards, R.L., Sinha, A., Spötl, C., Yi, L., Chen, S., Kelly, M., Kathayat, G., Wang, X., Li, X., Kong, X., Wang, Y., Ning, Y., Zhang, H., 2016b. The Asian monsoon over the past 640,000 years and ice age terminations. Nature 534, 640–646. https://doi.org/10.1038/nature18591.

Cheng, H., Spötl, C., Breitenbach, S.F.M., Sinha, A., Wassenburg, J.A., Jochum, K.P., Scholz, D., Li, X., Yi, L., Peng, Y., Lv, Y., Zhang, P., Votintseva, A., Loginov, V., Ning, Y., Kathayat, G., Edwards, R.L., 2016a. Climate variations of Central Asia on orbital to millennial timescales. Sci. Rep. 6, 36975. https://doi.org/10.1038/srep36975.

Cheng, H., Zhang, P.Z., Spötl, C., Edwards, R.L., Cai, Y.J., Zhang, D.Z., Sang, W.C., Tan, M., An, Z.S., 2012. The climatic cyclicity in semiarid-arid central Asia over the past 500,000 years. Geophys. Res. Lett. 39, L01705. https://doi.org/10.1029/2011GL050202.

Clark, P.U., Dyke, A.S., Shakun, J.D., Carlson, A.E., Clark, J., Wohlfarth, B., Mitrovica, J.X., Hostetler, S.W., McCabe, A.M., 2009. The last glacial maximum. Science 325, 710–714. https://doi.org/10.1126/science.1172873.

Curio, J., Maussion, F., Scherer, D., 2015. A 12-year high-resolution climatology of atmospheric water transport over the Tibetan Plateau. Earth Syst. Dyn. 6, 109–124. https://doi.org/10.5194/esd-6-109-2015.

Deplazes, G., Lückge, A., Peterson, L.C., Timmermann, A., Hamann, Y., Hughen, K.A., Röhl, U., Laj, C., Cane, M.A., Sigman, D.M., Haug, G.H., 2013. Links between tropical rainfall and North Atlantic climate during the last glacial period. Nat. Geosci. 6, 213–217. https://doi.org/10.1038/NGEO1712.

Disse, M., 2016. Sustainable land and water management of river oases along the Tarim River. Proc. Int. Assoc. Hydrol. Sci. (Proc. IAHS) 373, 25–29. https://doi.org/10.5194/piahs-373-25-2016.

Dong, W., Lin, Y., Wright, J.S., Ming, Y., Xie, Y., Wang, B., Luo, Y., Huang, W., Huang, J., Wang, L., Tian, L., Peng, Y., Xu, F., 2016. Summer rainfall over the southwestern Tibetan Plateau controlled by deep convention over the Indian subcontinent. Nat. Commun. 7, 10925. https://doi.org/10.1038/ncomms10925.

Dong, W., Lin, Y., Wright, J.S., Xie, Y., Xu, F., Xu, W., Wang, Y., 2017. Indian monsoon low-pressure systems feed up-and-over moisture transport to the southwestern Tibetan Plateau. J. Geophys. Res. Atmos. 122, 12,140–12,151. https://doi.org/10.1002/2017JD027296, 140-12,151.

Dutt, S., Gupta, A.K., Clemens, S.C., Cheng, H., Singh, R.K., Kathayat, G., Edwards, R.L., 2015. Abrupt changes in Indian summer monsoon strength during 33,800 to 5000 years B.P. Geophys. Res. Lett. 42, 5526–5532. https://doi.org/10.1002/2015GL064015.

Elmore, D., Tubbs, L.E., Newman, D., Ma, X.Z., Finkel, R., Nishiizumi, K., Beer, J., Oeschger, H., Andree, M., 1982. ^{36}Cl bomb pulse measured in a shallow ice core from Dye 3, Greenland. Nature 300, 735–737. https://doi.org/10.1038/300735a0.

Farinotti, D., Immerzeel, W.W., de Kok, R.J., Quincey, D.J., Dehecq, A., 2020. Manifestations and mechanisms of the Karakorum glacier anomaly. Nat. Geosci. 13, 8–16. https://doi.org/10.1038/s41561-019-0513-5.

Feng, S., Hu, Q., 2008. How the North Atlantic Multidecadal Oscillation may have influenced the Indian summer monsoon during the past two millennia. Geophys. Res. Lett. 35, L01707 https://doi.org/10.1029/2007GL032484.

Fleitmann, D., Burns, S.J., Mudelsee, M., Neff, U., Kramers, J., Mangini, A., Matter, A., 2003. Holocene forcing of the Indian Monsoon recorded in a stalagmite from Southern Oman. Science 300, 1737–1739. https://doi.org/10.1126/science.1083130.

Gasse, F., Arnold, M., Fontes, J.C., Fort, M., Gibert, E., Huc, A., Li, B., Li, Y., Liu, Q., Mélières, F., Van Campo, E., Wang, F., Zhang, Q., 1991. A 13,000-year climate record from western Tibet. Nature 353, 742–745. https://doi.org/10.1038/353742a0.

Goswami, B.N., Madhusoodanan, M.S., Neema, C.P., Sengupta, D., 2006. A physical mechanism for North Atlantic SST influence on the Indian summer monsoon. Geophys. Res. Lett. 33, L02706 https://doi.org/10.1029/2005GL024803.

Grootes, P.M., Stuvier, M., 1997. Oxygen 18/16 variability in Greenland snow and ice with 10^{-3} to 10^{5}-year time resolution. J. Geophys. Res.: Oceans 102, 26455–26470. https://doi.org/10.1029/97JC00880.

Gupta, A.K., Anderson, D.M., Overpeck, J.T., 2003. Abrupt changes in the Asian southwest monsoon during the Holocene and their links to the North Atlantic Ocean. Nature 421, 354–357. https://doi.org/10.1038/nature01340.

Han, X., Xue, H., Zhao, C., Lu, D., 2016. The roles of convective and stratiform precipitation in the observed precipitation trends in Northwest China during 1961-2000. Atmos. Res. 169, 139–146. https://doi.org/10.1016/j.atmosres.2015.10.001.

Hari, V., Villarini, G., Karmakar, S., Wilcox, L.J., Collins, M., 2020. Northward propagation of the Intertropical Convergence Zone and strengthening of the Indian summer monsoon. Geophys. Res. Lett. 47, e2020GL089823 https://doi.org/10.1029/2020GL089823.

Herzschuh, U., 2006. Palaeo-moisture evolution in monsoonal Central Asia during the last 50,000 years. Quat. Sci. Rev. 25, 163–178. https://doi.org/10.1016/j.quascirev.2005.02.006.

Hou, J., D'Andrea, W.J., Wang, M., He, Y., Liang, J., 2017. Influence of the Indian monsoon and the subtropical jet on climate change on the Tibetan Plateau since the late Pleistocene. Quat. Sci. Rev. 163, 84–94. https://doi.org/10.1016/j.quascirev.2017.03.013.

Hou, S., Jenk, T.M., Zhang, W., Wang, C., Wu, S., Wang, Y., Pang, H., Schwikowski, M., 2018. Age ranges of the Tibetan ice cores with emphasis on the Chongce ice cores, western Kunlun Mountains. Cryosphere 12, 2341–2348. https://doi.org/10.5194/tc-12-2341-2018.

Hou, S., Zhang, W., Pang, H., Wu, S., Jenk, T.M., Schwikowski, M., Wang, Y., 2019. Apparent discrepancy of Tibetan ice core δ^{18}O record may be attributed to misinterpretation of chronology. Cryosphere 13, 1743–1752. https://doi.org/10.5194/tc-13-1743-2019.

Huang, R., Zhu, H., Liang, E., Asad, F., Grießinger, J., 2019. A tree-ring-based summer (June-July) minimum temperature reconstruction for the western Kunlun Mountains since AD 1681. Theor. Appl. Climatol. 138, 673–682. https://doi.org/10.1007/s00704-019-02849-1.

Hudson, A.M., Quade, J., 2013. Long-term east-west asymmetry in monsoon rainfall on the Tibetan Plateau. Geology 41, 351–354. https://doi.org/10.1130/G33837.1.

Hugonnet, R., McNabb, R., Berthier, E., Menounos, B., Nuth, C., Girod, L., Farinotti, D., Huss, M., Dussaillant, I., Brun, F., Kääb, A., 2021. Accelerated global glacier mass loss in the early twenty-first century. Nature 592, 726–731. https://doi.org/10.1038/s41586-021-03436-z.

Jaglan, S., Gupta, A.K., Clemens, S.C., Dutt, S., Cheng, H., Singh, R.K., 2021. Abrupt Indian summer monsoon shifts aligned with Heinrich events and D-O cycles since MIS3. Palaeogeogr. Palaeoclimatol. Palaeoecol. 583, 110658 https://doi.org/10.1016/j.palaeo.2021.110658.

Johnsen, S.J., Dahl-Jensen, D., Gundestrup, N., Steffensen, J.P., Clausen, H.B., Miller, H., Masson-Delmotte, V., Sveinbjörnsdottir, A.E., White, J., 2001. Oxygen isotope and paleotemperatures records from six Greenland ice-core stations: Camp Century, Dye-3, GRIP, GISP2, Renland and NGRIP. J. Quat. Sci. 16, 299–307. https://doi.org/10.1002/jqs.622.

Ke, L., Ding, X., Song, C., 2015. Heterogenous changes of glaciers over the western Kunlun Mountains based on ICESat and Landsat-8 derived glacier inventory. Remote Sens. Environ. 168, 13–23. https://doi.org/10.1016/j.rse.2015.06.019.

Kellerhals, T., Brütsch, S., Sigl, M., Knüsel, S., Gäggelar, H.W., Schwikowski, M., 2010. Ammonium concentration in ice cores: a new proxy for regional temperature reconstruction? J. Geophys. Res. Atmos. 115, D16123 https://doi.org/10.1029/2009JD012603.

Kent, D.V., Hemming, S.R., Turrin, B.D., 2002. Laschamp excursion at Mono Lake? Earth Planet Sci. Lett. 197, 151–164. https://doi.org/10.1016/S0012-821X(02)00474-0.

Koriche, S.A., Nandini-Weiss, S.D., Prange, M., Singarayer, J.S., Arpe, K., Cloke, H.L., Schulz, M., Bakker, P., Leroy, S.A.G., Coe, M., 2021. Impacts of variations in Caspian Sea surface area on catchment-scale and large-scale climate. J. Geophys. Res. Atmos. 126, e2020JD034251 https://doi.org/10.1029/2020JD034251.

Koriche, S.A., Singarayer, J.S., Cloke, H.L., Valdes, P.J., Wesselingh, F.P., Kroonenberg, S.B., Wickert, A.D., Yanina, T.A., 2022. What are the drivers of Caspian Sea level variation during the late Quaternary? Quat. Sci. Rev. 283, 107457. https://doi.org/10.1016/j.quascirev.2022.107457.

Korte, M., Brown, M.C., Panovska, S., Wardinski, I., 2019. Robust characteristics of the Laschamp and Mono Lake geomagnetic excursions: results from global field models. Front. Earth Sci. 7, 86. https://doi.org/10.3389/feart.2019.00086.

Kraaijenbrink, P.D.A., Bierkens, M.F.P., Lutz, A.F., Immerzeel, W.W., 2017. Impact of global temperature rise of 1.5 degrees Celsius on Asia's glaciers. Nature 549, 257–260. https://doi.org/10.1038/nature23878.

Kreutz, K.J., Wake, C.P., Aizen, V.B., Cecil, L.D., Synal, H.-A., 2003. Seasonal deuterium excess in a Tien Shan ice core: influence of moisture transport and recycling in Central Asia. Geophys. Res. Lett. 30, 1922. https://doi.org/10.1029/2003GL017896.

Kutuzov, S., Thompson, L.G., Lavrentiev, I., Tian, L., 2018. Ice thickness measurements of Guliya ice cap, western Kunlun Mountains (Tibetan Plateau), China. J. Glaciol. 64 (248), 977–989. https://doi.org/10.1017/jog.2018.91.

Laj, C., Guillou, H., Kissel, C., 2014. Dynamics of the earth magnetic field in the 10-75 kyr period comprising the Laschamp and Mono Lake excursions: new results from the French Chaîne des Puys in a global perspective. Earth Planet Sci. Lett. 387, 184–197. https://doi.org/10.1016/j.epsl.2013.11.031.

Lascu, I., Feinberg, J.M., Dorale, J.A., Cheng, H., Edwards, R.L., 2016. Age of the Laschamp excursion determined by U-Th dating of a speleothem geomagnetic record from North America. Geology 44, 139–142. https://doi.org/10.1130/G37490.1.

Li, C.-G., Wang, M., Liu, W., Lee, S.-Y., Chen, F., Hou, J., 2021. Quantitative estimates of Holocene glacier meltwater variations on the Western Tibetan Plateau. Earth Planet Sci. Lett. 559, 116766 https://doi.org/10.1016/j.epsl.2021.116766.

Li, Y., Song, Y., Lai, Z., An, Z., 2016. Rapid and cyclic dust accumulation during MIS2 in Central Asia inferred from loess OSL dating and grain-size analysis. Sci. Rep. 6, 32365 https://doi.org/10.1038/srep32365.

Liu, J., Nowaczyk, N.R., Panovska, S., Korte, M., Arz, H.W., 2020. The Norwegian-Greenland Sea, the Laschamps, and the Mono Lake excursions recorded in a Black Sea sedimentary sequence spanning from 68.9 to 14.5 ka. J. Geophys. Res. Solid Earth 125, e2019JB019225. https://doi.org/10.1029/2019JB019225.

Liu, J., Wang, R., Zhao, Y., Yang, Y., 2019. A 40,000-year record of aridity and dust activity at Lop Nur, Tarim Basin, northwestern China. Quat. Sci. Rev. 211, 208–211. https://doi.org/10.1016/j.quascirev.2019.03.023.

Liu, Z., Zhu, J., Rosenthal, Y., Zhang, X., Otto-Bliesner, B.L., Timmermann, A., Smith, R.S., Lohmann, G., Zheng, W., Timm, O.E., 2014. The Holocene temperature conundrum. Proc. Natl. Acad. Sci. USA 111, E3501–E3505. https://doi.org/10.1073/pnas.1407229111.

Mankinen, E.A., Wentworth, C.M., 2004. Mono Lake excursion recorded in sediment of the Santa Clara valley, California. Geochem., Geophys., Geosys. 5, Q02H05. https://doi.org/10.1029/2003GC000592.

Marcott, S.A., Shakun, J.D., Clark, P.U., Mix, A.C., 2013. A reconstruction of regional and global temperature for the past 11,300 years. Science 339, 1198–1201. https://doi.org/10.1126/science.1228026.

Marzin, C., Kallel, N., Kageyama, M., Duplessy, J.-C., Braconnot, P., 2013. Glacial fluctuations of the Indian monsoon and their relationship with North Atlantic climate: new data and modelling experiments. Clim. Past 9, 2135–2151. https://doi.org/10.5194/cp-9-2135-2013.

Masson-Delmotte, V., Hou, S., Ekaykin, A., Jouzel, J., Aristarain, A., Bernardo, R.T., Bromwich, D., Cattani, O., Delmotte, M., Falourd, S., Frezzotti, M., Gallée, H., Genoni, L., Isaksson, E., Landais, A., Helsen, M.M., Hoffmann, G., Lopez, J., Morgan, V., Motoyama, H., Noone, D., Oerter, H., Petit, J.R., Royer, A., Uemura, R., Schmidt, G.A., Schlosser, E., Simões, J.C., Steig, E.J., Stenni, B., Stievenard, M., van den Broeke, van de Wal, R.S.W., van de Berg, W.J., Vimeux, F., White, J.W.C., 2008. A review of Antarctic surface snow isotopic composition: observations, atmospheric circulation, and isotopic modeling. J. Clim. 21, 3359–3387. https://doi.org/10.1175/2007JCLI2139.1.

Maussion, F., Scherer, D., Mölg, T., Collier, E., Curio, J., Finkelnburg, R., 2014. Precipitation seasonality and variability over the Tibetan Plateau as resolved by the High Asia reanalysis. J. Clim. 27, 1910–1927. https://doi.org/10.1175/JCLI-D-13-00282.1.

Mayewski, P.A., Bender, M., 1995. The GISP2 ice core record-Paleoclimate highlights. Rev. Geophys. 33, 1287–1296. https://doi.org/10.1029/95RG00498.

Monnin, E.A., Steig, E.J., Siegenthalar, U., Kawamura, K., Schwander, J., Stauffer, B., Stocker, T.F., Morse, D.L., Barnola, J.-M., Bellier, B., Raynaud, D., Fischer, H., 2004. Evidence for substantial accumulation rate variability in Antarctica during the Holocene, through synchronization of CO_2 in the Taylor Dome, Dome C and DML ice cores. Earth Planet. Sci. Lett. 224, 45–54. https://doi.org/10.1016/j.epsl.2004.05.007.

Muscheler, R., Beer, J., Kubik, P.W., Synal, H.-A., 2005. Geomagnetic field intensity during the last 60,000 years based on ^{10}Be and ^{36}Cl from the Summit ice cores and ^{14}C. Quat. Sci. Rev. 24, 1849–1860. https://doi.org/10.1016/j.quascirev.2005.01.012.

Nilsson, A., Muscheler, R., Snowball, I., Aldahan, A., Possnert, G., Augustinus, P., Atkin, D., Stephens, T., 2011. Multi-proxy identification of the Laschamp geomagnetic field excursion in Lake Pupuke, New Zealand. Earth Planet Sci. Lett. 311, 155–164. https://doi.org/10.1016/j.epsl.2011.08.050.

Paillard, D., Labeyrie, L., You, P., 1996. Analyseries 1.0: a Macintosh software for the analysis of geographical time-series. Eos 77, 379.

Pan, Y.X., Zhu, R.X., Liu, Q.S., Guo, B., Yue, L.P., Wu, H.N., 2002. Geomagnetic episodes of the last 1.2 Myr recorded in Chinese loess. Geophys. Res. Lett. 29, 1282. https://doi.org/10.1029/2001GL014024.

Pang, H., Hou, S., Zhang, W., Wu, S., Jenk, T.M., Schwikowski, M., Jouzel, J., 2020. Temperature trends in the northwestern Tibetan Plateau constrained by ice core water isotopes over the past 7,000 years. J. Geophys. Res. Atmos. 125, e2020JD032560 https://doi.org/10.1029/2020JD032560.

Pang, Z., Kong, Y., Froehlich, K., Huang, T., Yuan, L., Li, Z., Wang, F., 2011. Processes affecting isotopes in precipitation of an arid region. Tellus B 63, 352–359. https://doi.org/10.1111/j.1600-0889.2011.00532.x.

Panovska, S., Korte, M., Liu, J., Nowaczyk, N., 2021. Global evolution and dynamics of the geomagnetic field in the 15-70 kyr period based on selected paleomagnetic sediment records. J. Geophys. Res. Solid Earth 126, e2021JB022681. https://doi.org/10.1029/2021JB022681.

Pritchard, H.D., 2019. Asia's shrinking glaciers protect large populations from drought stress. Nature 569, 649–654. https://doi.org/10.1038/s41586-019-1240-1.

Raisbeck, G.M., Cauquoin, A., Jouzel, J., Landais, A., Petit, J.-R., Lipenkov, V.Y., Beer, J., Synal, H.-A., Oerter, H., Johnsen, S.J., Steffensen, J.P., Svensson, A., Yiou, F., 2017. An improved north-south synchronization of ice core records around the 41 kyr ^{10}Be peak. Clim. Past 13, 217–229. https://doi.org/10.5194/cp-13-217-2017.

Ramisch, A., Lockot, G., Haberzettl, T., Hartmann, K., Kuhn, G., Lehmkuhl, F., Schimpf, S., Schulte, P., Stauch, G., Wang, R., Wünnemann, B., Yan, D., Zhang, Y., Diekmann, B., 2016. A persistent northern boundary of Indian summer monsoon precipitation over Central Asia during the Holocene. Sci. Rep. 6, 25791. https://doi.org/10.1038/srep25791.

Roberts, A.P., 2008. Geomagnetic excursions: knowns and unknowns. Geophys. Res. Lett. 35, L17307 https://doi.org/10.1029/2008GL034719.

Routson, C.C., McKay, N.P., Kaufman, D.S., Erb, M.P., Goosse, H., Shuman, B.N., Rodysill, J.R., Ault, T., 2019. Mid-latitude net precipitation decreased with Arctic warming during the Holocene. Nature 568, 83–87. https://doi.org/10.1038/s41586-019-1060-3.

Schiemann, R., Lüthi, D., Schär, C., 2009. Seasonality and interannual variability of the Westerly jet in the Tibetan Plateau region. J. Clim. 22, 2940–2957. https://doi.org/10.1175/2008JCLI2625.1.

Svensson, A., Andersen, K.K., Bigler, M., Clausen, H.B., Dahl-Jensen, D., Davies, S.M., Johnsen, S.J., Muscheler, R., Rasmussen, S.O., Röthlisberger, R., Steffensen, J.P., Vinther, Bo.M., 2006. The Greenland ice core chronology 2005, 15-42 ka Part 2: comparison to other records. Quat. Sci. Rev. 25, 3258–3267. https://doi.org/10.1016/j.quascirev.2006.08.003.

Thomas, E.K., Huang, Y., Clemens, S.C., Colman, S.M., Morrill, C., Wegener, P., Zhao, J., 2016. Changes in dominant moisture sources and the consequences for hydroclimate on the northeastern Tibetan Plateau during the past 32 kyr. Quat. Sci. Rev. 131, 157–167. https://doi.org/10.1016/j.quascirev.2015.11.003.

Thompson, L.G., Mosley-Thompson, E., Brecher, H., Davis, M., León, B., Les, D, Lin, P.-N., Mashiotta, T., Mountain, K., 2006. Abrupt tropical climate change: past and present. Proc. Natl. Acad. Sci. U.S.A. 103, 10536–10543. https://doi.org/10.1073/pnas.0603900103.

Thompson, L.G., Severinghaus, J.P., Yao, T., Davis, M.E., Mosley-Thompson, E., Beaudon, E., Sierra-Hernández, M.R., Porter, S.E., 2022. Use of $\delta^{18}O_{atm}$ in dating a Tibetan ice core record of Holocene/Late Glacial climate. Proc. Natl. Acad. Sci. U.S.A. 119, e2205545119 https://doi.org/10.1073/pnas.2205545119.

Thompson, L.G., Yao, T., Davis, M.E., Henderson, K.A., Yao, T., Davis, M.E., Henderson, K.A., Mosley-Thompson, E., Lin, P.-N., Beer, J., Synal, H.-A., Cole-Dai, J., Bolzan, J.F., 1997. Tropical climate instability: the last glacial cycle from a Qinghai-Tibetan ice core. Science 276, 1821–1825. https://doi.org/10.1126/science.276.5320.1821.

Thompson, L.G., Yao, T., Davis, M.E., Mosley-Thompson, E., Wu, G., Porter, S.E., Xu, B., Lin, P.-N., Wang, N., Beaudon, E., Duan, K., Sierra-Hernández, M.R., Kenny, D.V., 2018. Ice core records of climate variability on the Third Pole with emphasis on the Guliya ice cap, western Kunlun Mountains. Quat. Sci. Rev. 188, 1–14. https://doi.org/10.1016/j.quascirev.2018.03.003.

Tian, L., Yao, T., Li, Z., MacClune, K., Wu, G., Xu, B., Li, Y., Lu, A., Shen, Y., 2006. The recent rapid warming trend revealed from the isotopic record in Muztagata ice core, eastern Pamirs. J. Geophys. Res. 111, D13103. https://doi.org/10.1029/2005JD006249.

Tian, L., Yao, T., MacClune, K., White, J.W.C., Schilla, A., Vaughn, B., Vachon, R., Ichiyanagi, K., 2007. Stable isotopic variations in west China: a consideration of moisture sources. J. Geophys. Res. Atmos. 112, D10112. https://doi.org/10.1029/2006JD007718.

Tian, L., Yao, T., Schuster, P.F., White, J.W.C., Ichiyanagi, K., Pendall, E., Pu, J., Yu, W., 2003. Oxygen-18 concentrations in recent precipitation and ice cores on the Tibetan Plateau. J. Geophys. Res. 108, 4293. https://doi.org/10.1029/2002JD002173.

Tierney, J.E., Pausata, F.S.R., deMenocal, P., 2016. Deglacial Indian monsoon failure and North Atlantic stadials linked by Indian Ocean surface cooling. Nat. Geosci. 9, 46–50. https://doi.org/10.1038/NGEO2603.

Vuille, M., Werner, M., Bradley, R.S., Keiming, F., 2005. Stable isotopes in precipitation in the Asian monsoon region. J. Geophys. Res. 110, D23108 https://doi.org/10.1029/2005JD006022.

Wagner, G., Beer, J., Laj, C., Kissel, C., Masarik, J., Muscheler, R., Synal, H.-A., 2000. Chlorine-36 evidence for the Mono Lake event in the Summit GRIP ice core. Earth Planet Sci. Lett. 181, 1–6. https://doi.org/10.1016/S0012-821X(00)00196-5.

Wang, N., Yao, T., Thompson, L.G., Davis, M.E., 2006. Strong negative correlation between dust event frequency and air temperature over the northern Tibetan Plateau reflected by the Malan ice-core record. Ann. Glaciol. 43, 29–33. https://doi.org/10.3189/172756406781812339.

Xu, X., Tan, X., Yu, G., Wu, G., Fang, W., Chen, J., Song, H., Shen, J., 2013. Normal- and oblique-slip of the 2008 Yutian earthquake: evidence for eastward block motion, northern Tibetan Plateau. Tectonophysics 584, 152–165. https://doi.org/10.1016/j.tecto.2012.08.007.

Yang, X., Preusser, F., Radtke, U., 2006. Late Quaternary environmental changes in the Taklamakan Desert, western China, inferred from OSL-dated lacustrine and aeolian deposits. Quat. Sci. Rev. 25, 923–932. https://doi.org/10.1016/j.quascirev.2005.06.008.

Yang, X., Scuderi, L., Paillou, P., Liu, Z., Li, H., Ren, X., 2011. Quaternary environmental changes in the drylands of China-A critical review. Quat. Sci. Rev. 30, 3219–3233. https://doi.org/10.1016/j.quascirev.2011.08.009.

Yao, T., Masson-Delmotte, V., Gao, J., Yu, W., Yang, X., Risi, C., Sturm, C., Werner, M., Zhao, H., He, Y., Ren, W., Tian, L., Shi, C., Hou, S., 2013. A review of climate controls on δ18O in precipitation over the Tibetan Plateau: Observations and simulations. Rev. Geophys. 51, 525–548. https://doi.org/10.1002/rog.20023.

Yao, T., Thompson, L., Yang, W., Yu, W., Gao, Y., Guo, X., Yang, X., Duan, K., Zhao, H., Xu, B., Pu, J., Lu, A., Xiang, Y., Kattel, D.B., Joswiak, D., 2012. Different glacier status with atmospheric circulations in Tibetan Plateau and surroundings. Nat. Clim. Change 2, 663–667. https://doi.org/10.1038/nclimate1580.

Yao, T., Thompson, L.G., Chen, D., Zhang, Y., Wang, N., Zhao, L., Che, T., Xu, B., Wu, G., Zhang, F., Tang, Q., Immerzeel, W., Bolch, T., Pellicciotti, F., Li, X., Yang, W., Gao, J., Wang, W., 2020. Third Pole warming and cryosphere system changes. World Meteorol. Organ. Bull. 69 (1), 38–44.

Yao, T., Thompson, L.G., Mosley-Thompson, E., Yang, Z., Zhang, X., Lin, P.-N., 1996. Climatological significance of δ^{18}O in north Tibetan ice cores. J. Geophys. Res. Atmos. 101, 29531–29537. https://doi.org/10.1029/96JD02683.

Yu, G., Gui, F., Shi, Y., Zheng, Y., 2007. Late marine isotope stage 3 palaeoclimate for East Asia: a data-model-comparison. Palaeogeogr. Palaeoclimatol. Palaeoecol. 250, 167–183. https://doi.org/10.1016/j.palaeo.2007.03.010.

Yu, W., Yao, T., Thompson, L.G., Jouzel, J., Zhao, H., Xu, B., Jing, Z., Wang, N., Wu, G., Ma, Y., Gao, J., Yang, X., Zhang, J., Qu, D., 2021. Temperature signals of ice core and speleothem isotopic records from Asian monsoon region as indicated by precipitation δ^{18}O. Earth Planet Sci. Lett. 554, 116665. https://doi.org/10.1016/j.epsl.2020.116665.

Zhang, C., Zhao, C., Yu, S.-Y., Yang, X., Cheng, J., Zhang, X., Xue, B., Shen, J., Chen, F., 2022a. Seasonal imprint of Holocene temperature reconstruction of the Tibetan Plateau. Earth Sci. Rev. 226, 103927 https://doi.org/10.1016/j.earscirev.2022.103927.

Zhang, S., Zhao, H., Sheng, Y., Zhang, J., Sun, A., Wang, L., Huang, L., Hou, J., Chen, F., 2022b. Mega-lakes in the northwestern Tibetan Plateau formed by melting glaciers during the last deglacial. Quat. Sci. Rev. 285, 107528 https://doi.org/10.1016/j.quascirev.2022.107528.

Zhang, X., Zhou, A., Zhang, C., Hao, S., Zhao, Y., An, C., 2016. High-resolution records of climate change in arid eastern Central Asia during MIS 3 (51 600-25 300 cal a BP) from Wulungu Lake, north-western China. J. Quat. Sci. 31, 577–586. https://doi.org/10.1002/jqs.2881.

Zhou, J., Wu, J., Zhang, H., Zeng, H., Shen, B., 2022. Late Quaternary hydroclimate change inferred from lake sedimentary record in arid central Asia. Boreas 51, 573–583. https://doi.org/10.1111/bor.12573.

Zhou, W., Priller, A., Beck, J.W., Wu, Z., Chen, M., An, Z., Kutschera, W., Xian, F., Yu, H., Liu, L., 2007. Disentangling geomagnetic and precipitation signals in an 80-kyr Chinese loess record of ^{10}Be. Radiocarbon 49, 137–158. https://doi.org/10.1017/S0033822200041977.

Zhu, L., Lü, X., Wang, J., Peng, P., Kasper, T., Daut, G., Haberzettl, T., Frenzel, P., Li, Q., Yang, R., Schwalb, A., Mäusbacher, R., 2015. Climate change on the Tibetan Plateau in response to shifting atmospheric circulation since the LGM. Sci. Rep. 5, 13318. https://doi.org/10.1038/srep13318.

Zhu, M., Thompson, L.G., Zhao, H., Yao, T., Yang, W., Jin, S., 2021. Influence of atmospheric circulation on glacier mass balance in Western Tibet: An analysis based on observations and modeling. J. Clim. 34, 6743–6757. https://doi.org/10.1175/JCLI-D-20-0988.s1.

Zhu, M., Yao, T., Yang, W., Wu, G., Li, S., Zhao, H., Thompson, L.G., 2022. Possible causes of anomalous glacier mass balance in the western Kunlun Mountains. J. Geophys. Res. Atmos. 127, e2021JD035705 https://doi.org/10.1029/2021JD035705.

Zweck, C., Huybrechts, P., 2005. Modeling of the northern hemisphere ice sheets during the last glacial cycle and glaciological sensitivity. J. Geophys. Res. Atmos. 110, D07103 https://doi.org/10.1029/2004JD005489.